AUTOMATION BASED ON KNOWLEDGE MODELING THEORY AND ITS APPLICATIONS IN ENGINE DIAGNOSTIC SYSTEMS USING SPACE SHUTTLE MAIN ENGINE VIBRATIONAL DATA

by

JONNATHAN H. KIM

A THESIS

Submitted in partial fulfillment of the requirements
for the degree of Electrical Engineering in
the Department of Electrical Engineering
of
The School of Graduate Studies
of
The University of Alabama in Huntsville

HUNTSVILLE, ALABAMA

1995

THESIS APPROVAL FORM

Submitted by Jonnathan H. Kim in partial fulfillment of the requirements for the degree of Master of Science with a major in Electrical Engineering.

Accepted on behalf of the Faculty of the School of Graduate Studies by the thesis committee:

_____ Committee Chair

(Date)

_____

_____

_____ Department Chair

_____ College Dean

_____ Graduate Dean

ABSTRACT

Humans can perform many complicated tasks without explicit rules. This inherent and advantageous capability becomes a hurdle when a task is to be automated. Modern computers and numerical calculations require explicit rules and discrete numerical values. In order to bridge the gap between human knowledge and automating tools, a knowledge model is proposed. Knowledge modeling techniques are discussed and utilized to automate a labor and time intensive task of detecting anomalous bearing wear patterns in the Space Shuttle Main Engine (SSME) High Pressure Oxygen Turbopump (HPOTP).

ACKNOWLEDGEMENTS

I want to thank my Masters program advisory committee including Dr. Porter, Dr. Epperson, and Dr. Stensby. I would like to extend special thanks to Mr. Tom Zoladz of Marshall Space Flight Center(MSFC), NASA, for providing valuable expertise and data. My appreciation also goes to Mr. Ralph Kissel (MSFC/NASA) who provided assistance as my co-investigator on a Center Director's Discretionary Fund (CDDF) research project at NASA/MSFC.

This research was partially supported by Center Director's Discretionary Fund at NASA/MSFC in Huntsville, AL during the period of 1991 - 1993.

TABLE OF CONTENTS

LIST OF ILLUSTRATIONS

Chapter I

INTRODUCTION

Imagine a futuristic house without mundane chores: no more mowing, weekend car maintenance, plumbing repairs, etc. Imagine an automated system that performs all these dreaded chores with a push of a button. What a great dream!

To appreciate the intricate processes for automating these chores, let's look at a fairly simple task that many of us perform, for example, mowing. Mowing may seem like an innocuous task, but it involves many complicated design issues. One design issue involves path planning, i.e. how to efficiently cut the desired area without leaving uncut patches. The path planning should incorporate collision avoidance and terrain management. Object recognition should be implemented. How does a mower identify different debris and objects, and then make a decision to mow right through the object or to avoid the object? How does it compensate for uneven terrain with pot holes and severe slopes? This example illustrates complexities of an automated task. Even a simple task such as mowing takes extensive efforts to automate.

However, if the difficulties of automation can be overcome, the benefits can be enormous. Cost reductions and time savings can be achieved. Human operators can be freed from mundane labor-intensive tasks.

This document lays out a theoretical background on knowledge modeling. Specifically, this document deals with techniques that could be used to automate tasks that are currently performed manually by human operators. A knowledge model is proposed, and a series of techniques are discussed for automation. Based on knowledge models and techniques, an automated data analyzer is implemented for the Space Shuttle Main Engine (SSME) vibrational data.

Chapter 2

BACKGROUND

A. Definition of Knowledge

In this document, a definition of knowledge is proposed from the perspective of a knowledge acquirer, a person who gathers information from experts. By use of the definition, a knowledge model is developed and implemented.

If a task is performed with a conscious intention, then it is said that knowledge is available for the task. If a person hits a golf ball with an intention of hitting the ball, there is available knowledge for the hitting task. If a person hits a ball accidentally off the tee, then there may not be knowledge available for the mishap. If the available knowledge can be described in any physical means, written, demonstrable, verbal, or other means, then the knowledge is defined as *accessible*. If the knowledge is subconscious and cannot be described, the knowledge is said to be *inaccessible*. Accessible knowledge can be further divided into explicitly accessible and implicitly accessible. *Explicitly accessible* knowledge can be executed by other humans, computers, and devices with the exact same results. *Implicitly accessible* knowledge results in similar outcomes when performed by different operators.

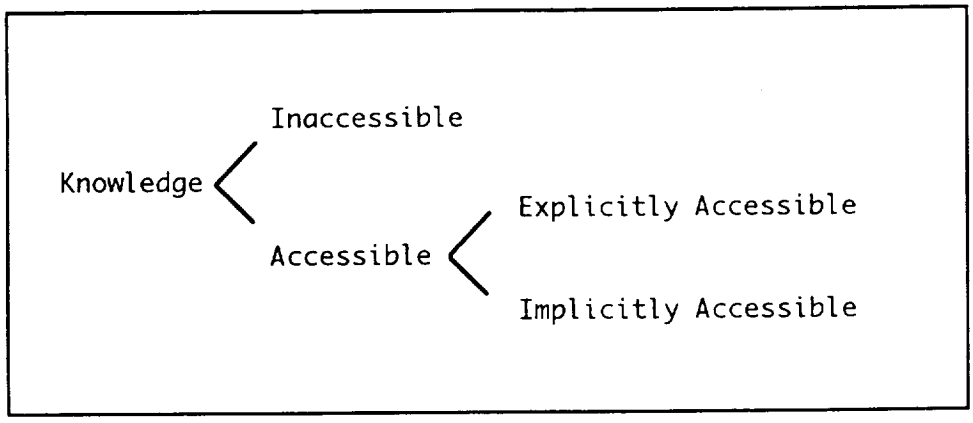

Figure 2.1 Knowledge Definition

For example, the multiplication table represents explicitly accessible knowledge. Written musical notes are also explicitly accessible knowledge. These are explicitly accessible since these tasks using this knowledge will result in exactly the same results. Two times five is ten. Whether a calculator performs the task, or an individual does it, the result should be the same. If a piece of music score is copied, the exact same results are achieved. A quarter note in C will be copied onto a music sheet as the same.

However, the real world is not multiples of integers or a series of quarter notes. The real world rarely can be modeled using explicit notations and formulas. Implicitly accessible knowledge describes a large domain of human knowledge. Implicitly accessible knowledge, when executed, results in similar outcomes. Buying two apples at a grocery store by different individuals will result in similar outcomes. Rather than making a long specification of exact weight, size, and color, the requirements are reduced to having two apples without sacrificing the main objective. Driving a car at 55 miles per hour (mph) implies driving a car at approximately 55 mph. If the actual speed was 54.1 or 55.6, in most cases, the objective is achieved.

Unlike the above examples, some domains of knowledge may not be accessible. Often athletes talk of 'feel for the shots' and 'being in the zone.' All these lingoes describe combinations of psychological, physiological, and neuromuscular states that are hard to describe. If a tennis player was asked to describe the feel of a successful top-spin forehand, the player would be at a loss for words. In order to teach an athlete to acquire the feel, an instructor may have to demonstrate the physical attributes. A description of cause and effect may have to be explained as well. This type of knowledge description is rather indirect in nature. Using indirect characterization such as cause-and-effect and other attributes, knowledge can be descibed to another individual.

The boundaries of these knowledge classes vary based on very subjective criteria, such as the participants' expertise, prior experiences, context, etc. What may seem to be quite accessible to one person may not be accessible to another person at all. It is also possible for a certain piece of knowledge to move and become another class of knowledge. Accessible knowledge becomes inaccessible as the person becomes more familarized with the task [Kidd, Welbank, 1984].

Humans have an innate capacity to process accessible and inaccessible knowledge to perform various activities without conscious realization of the processes. When we perform tasks without conscious realization, it becomes very difficult to

develop a link between the human knowledge and machine knowledge. Automation of manual tasks is feasible when human knowledge can be translated into the computer domain and language. Then, how do we bridge the human knowlege and the computer system? The next section proposes some knowlege modeling techniques.

B. Knowledge Modeling

This section describes the various types of knowledge modeling techniques.

1. Explicit Knowledge Modeling

a. Bi-level logic modeling

This is a True/False type of representation. '*5.1 is greater than 5.0.*' This statement can be regarded as a True/False statement. There is an explicit relationship already defined by what is meant by 'greater.' Furthermore, the statement has a definite truth/falsity assigned to it. A truth table can be constructed using bi-level logic.

b. Notational modeling

By using explicit notations (mathematical symbols, musical notes, etc.), it is possible to model explicitly accessible knowledge. Mathematics utilizes explicit notations for operators and operands. Musical notes are also explicitly expressed. A line with the slope 2 and intercept 5 in a 2-dimensional space can be expressed as '$y = 2x + 5$.' This equation of a line is a representation using *explicit* mathematical terms.

2. Implicit Knowledge Modeling

One technique to model implicit knowledge is to employ continuous logic (sometimes called analog logic). Continuous logic can be viewed as a superset of bi-level logic. In the domain of continuous logic, knowledge is modeled via pseudo-continuous level membership. One example would be fuzzy logic that models linguistic expression such as *slow, fast, hard* and *soft*. For example, in an expression,'*It is raining hard.* ', the word 'hard' is understood qualitatively, not with

explicit numbers such as 5.0 inches per hour. This is considered an *implicit* knowledge representation technique. The meaning of *hardness* varies with individual cases, but in this context *hard rain* is an understood situation. Analog logic and fuzzy systems allow mapping of a large sector of human knowledge to numerically definable representations.

3. Inaccessible knowledge modeling

One modeling technique that is well suited for inaccessible knowledge is a class of biololgically motivated modeling techniques. These biologically motivated modeling techniques are developed based on biological, physiological, and psychological environments. The most well-known case in the development of biologically-motivated modeling is Artificial Neural Networks (ANNs). Artificial Neural Networks are based on artificial neurons which consist of a summation node and a non-linear threshold function (see Figure 2.2). The output of the jth neuron, O_j, is

$$O_j = \text{Thr} \left(\sum_n I_n W_n\right),$$

where Thr is a threshold function.

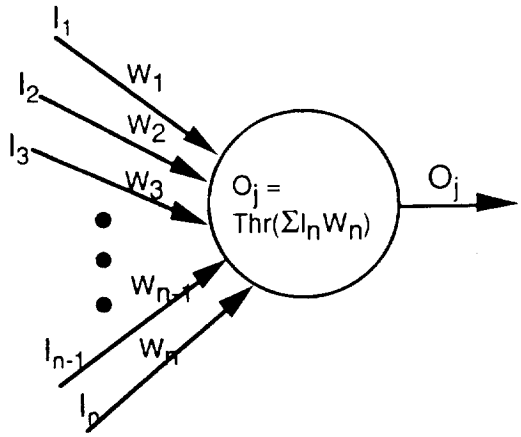

Figure 2.2 Artificial Neuron

Using layers (or slabs) of artificial neurons, an ANN can learn complex non-linear transfer functions. A typical ANN may look like Figure 2.3.

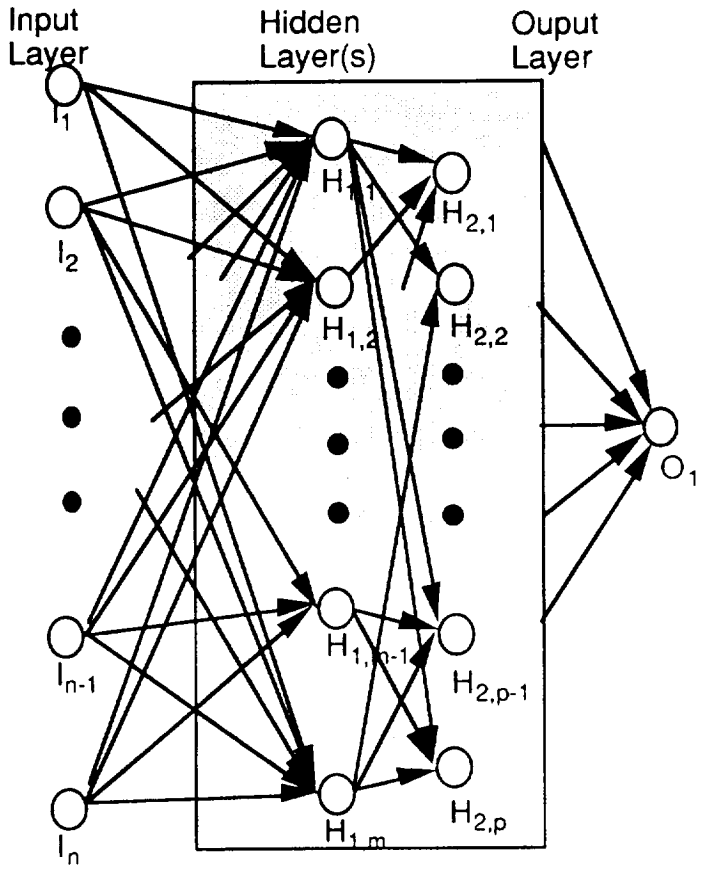

Figure 2.3. Artificial Neural Networks

The biologically motivated modeling techniques have been used to classify and to model many phenomena that are not easily modeled otherwise. For example, ANN's ability to learn without explicit instruction can be used to model inaccessible knowledge.

Chapter III

PROBLEM STATEMENT

A. Selection of Test Case

In order to implement an automated system and to prove feasibility, a set of criteria was determined to select a candidate system. These criteria were:

Real Case - The test should be based on a real application, not simulation alone.
Human Knowledge Availability - There is existing human knowledge or experts in the field.
Data Availability - Data is readily available for tests and verification.
Potential Benefits - Benefits can be realized in the near future and can be proved to enhance existing approaches.
Feasibility - The task should not require inordinate cost and time.

Two cases were investigated for its potential benefits. One was a keyboard entry device using Electroencephalogram (EEG) data. This type of device could be used for quadriplegics. However, data acquisition using human subjects became questionable. Furthermore, the need for a fairly complicated data acquisition unit was another deterrent. The second candidate was Space Shuttle Main Engine (SSME) diagnostics. This seemed to fit all criteria well. There is human expertise available, yet the expertise has been very difficult to document and to automate. A massive amount of engine data is available locally at NASA/Marshall Space Flight Center via computer network. Furthermore, automating such tasks can result in significant reduction of man-power and time.

B. Space Shuttle Main Engine Diagnostics

1. Background

During the development of the Space Shuttle Main Engine (SSME), significant progress has been made in both NASA and the aerospace communities in improving the diagnostic evaluation of high frequency dynamic data. Fast and reliable evaluation of such data is crucial to the Space Shuttle Operations program for preventing catastrophic engine hardware failures; moreover, reliable diagnostic evaluations can extend scheduled maintenance intervals of major components such as the high-speed turbopumps. Dynamic assessment of the SSME is very challenging due to the computational and manpower intensive nature of the data acquisition and signal processing operations. Furthermore, the acquired dynamic signatures taken from various locations throughout the engine system can be very complex to analyze. Current SSME dynamic data processing and evaluation are performed post-flight or following ground test with a typical diagnostic turnaround time of approximately one day. This primary evaluation can be improved upon significantly by automating manual analysis tasks.

One such task involves the evaluation of SSME High Pressure Oxygen Turbopump (HPOTP) dynamic data for bearing distress frequency content. The primary failure mode for HPOTP bearings is uneven ball wear, and the existence of cage frequency components in HPOTP is used to detect the characteristic bearing defect. Searching for cage frequency is difficult due to the character of the SSME HPOTP dynamic environment as sensed by the externally mounted accelerometers and strain guages. Analysts must frequently contend with structural, combustion, and electronically generated noise which mask the cage indicators. Also, feedthroughs from the other three SSME turbopumps must be considered. When wear indication is observed by the externally mounted transducers, substantial ball wear has already taken place. Therefore, any indication of bearing cage or cage harmonic frequency content in SSME HPOTP dynamic data is justification for removing the unit from the flight inventory.

Spectrograms, commonly referred to as waterfall plots, are often used to detect cage frequencies in high frequency dynamic data

channels. The cage frequency, along with subsequent harmonics, reflect nonuniform bearing rolling element diameters[Hine, 1989]. However, monitored HPOTP dynamic data channels frequently contain several other discrete and random narrow-band components which can coexist or mask predicted cage frequency signal content. synchronous frequency (SF), i.e., fundamental rotor speed, and its harmonics along with structural and hydrodynamic signals contribute to the noise.

Decisions made by analysts are determined by their ability to distinguish anomalous cage frequencies. Locations of cage and synchronous frequencies, and their relations to the thrust level changes are understood by analysts based on past experiences. An analyst may look for cage frequencies without complicated numerical computations by simply scanning the hard copies. Occasionally this type of subjective decision making results in differences in opinions among analysts.

2. Preliminary Analysis

To further illustrate the decision process, two cases of actual engine data are presented. The first case is data with anomalous cage frequency as shown in Figure 3.1, where the x and y axes denote frequency (in Hz) and time (in frame counts) respectively. The cage frequency is determined by a method described as below:

Inspecting the plot at approximately 450 Hz, one can locate a series of very prominent peaks. These peaks are the representation of the synchronous frequency (SF). The SF is used to find cage frequencies. 2C (2nd harmonic cage frequency) is found as a series of peaks between 390 Hz to 410 Hz (approximately 2 x 0.43 x SF). [McFadden, Smith, 1983]. As the thrust level changes, SF changes in proportion. The peak train at approximately 590 Hz is feedthrough from the High Pressure Fuel Turbopump, and can sometimes be confused for 3C (3rd harmonic cage frequency) data.

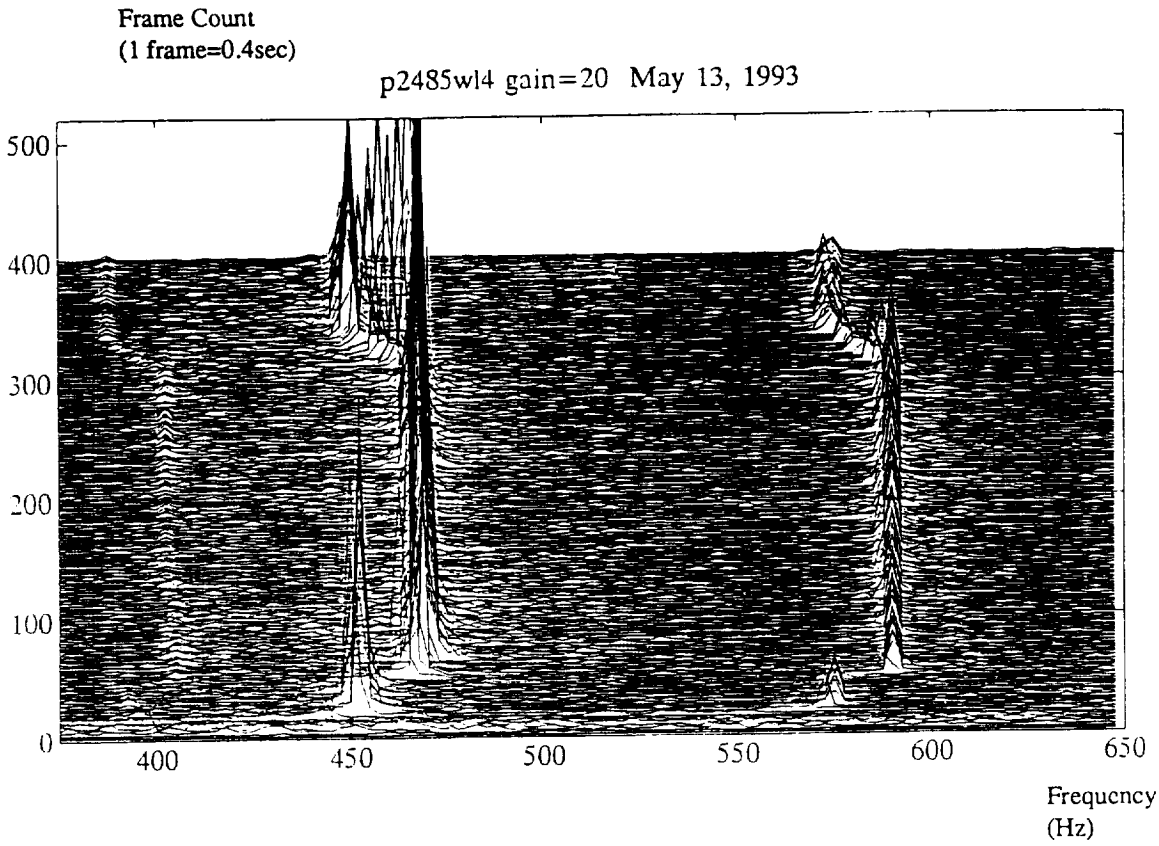

Figure 3.1 Anomalous Case (2485wl45)

The second case, as shown in Figure 3.2, is a nominal case. A similar procedure is used to determine its health. The SF is located and cage frequency is searched for. Unlike the abnormal case, there are no consistent peaks that vary with the SF. The same procedure is repeated to find the harmonics of the cage frequency. This case is found to have no anomalous peaks at any cage frequencies.

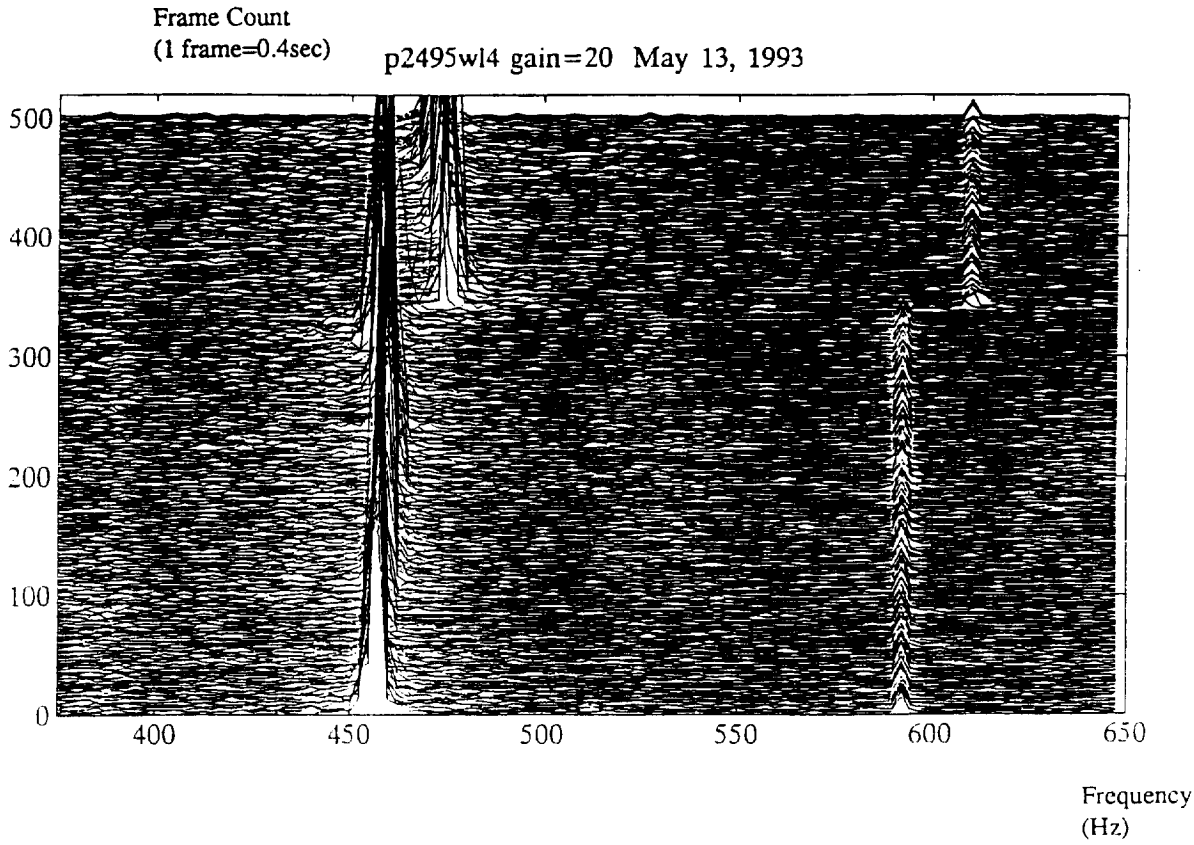

Figure 3.2 Nominal Case (2495wl45)

Chapter IV

IMPLEMENTATION AND RESULTS

The knowledge definition and the classification given above allow a coherent method to manage human expertise and to automate the expertise. Using this definition of knowledge, human expertise described in the problem statement, Section 2 of Chapter III, can be classified in the following manner.

Explicitly Accessible Knowledge:

Discrete Fourier Transform

Implicitly Accessible Knowledge:

Location of the synchronous frequency and its harmonics,
Location of the cage frequency and its harmonics,
Thrust level and its affects on synchronous frequency.

Inaccessible Knowledge:

Detection of anomalous peaks in spectral plots.

Further analysis of the human expertise allows a breakdown of the task into smaller and simpler sequential tasks as shown in Figure 4.1.

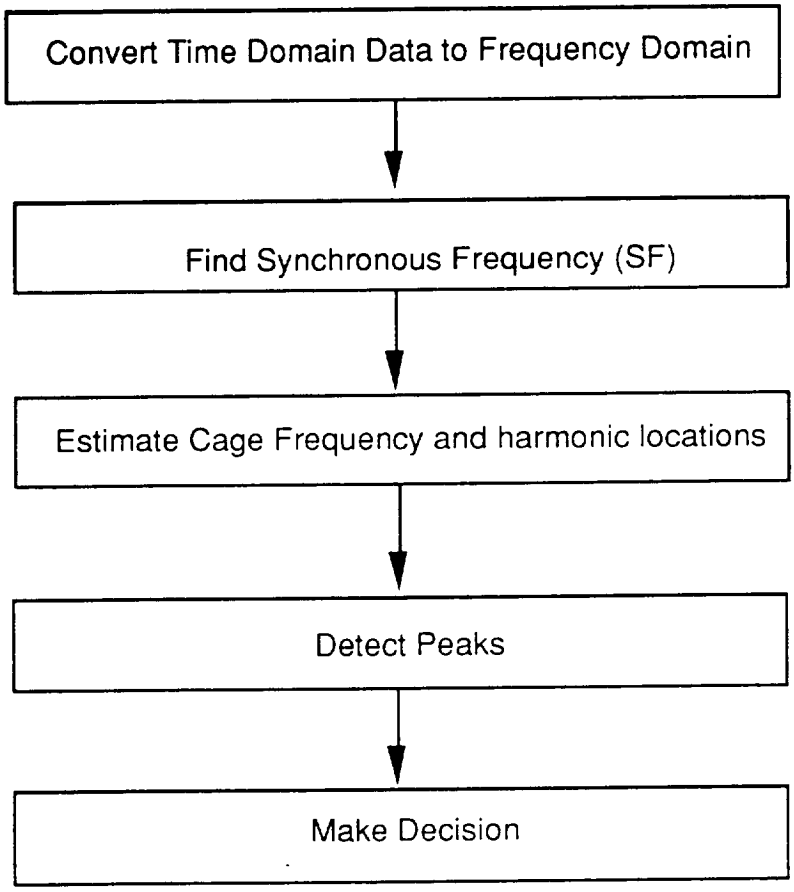

Figure 4.1. Sequential Breakdown of the Expertise

Twelve data files were provided by the Structural Dynamics Laboratory at Marshall Space Flight Center. These time-domain binary files contained vibrational engine data sampled at 10,240 Hz.

A. Discrete Fourier Transform

The Discrete Fourier Transform defines the relationship between the time domain data and its representation in the frequency domain. The definition of the Fourier transform of a continuous signal x(t) is defined as:

$$X(f) = F\{x(t)\} = \int_{-\infty}^{+\infty} x(t)\exp(-j2\pi ft)dt$$

The inverse transform is defined as:

$$x(t) = F^{-1}\{X(f)\} = \int_{-\infty}^{+\infty} X(f)\exp(j2\pi ft)df$$

These valuable relationships deal with continuous infinite length and infinitely many harmonically related complex exponentials. These relationships can be extended to sampled data. For a sequence of data that is uniformly sampled, The Discrete Fourier Transform can be used efficiently. For Discrete Fourier Transforms (DFT), the following equations are used:

Analysis Equation: $X[k] = \sum_{n=0}^{N-1} x[n]W_N^{kn}$

Synthesis Equation: $x[n] = (1/N)\sum_{k=0}^{N-1} X[k]W_N^{-kn}$

where $W_N = e^{-j(2\pi/N)}$

The relationship between frequency resolution, df, size of frame, N, and sampling time interval, dt, is defined as:

df = 1/ (N x dt)

Since the engine vibrational data is sampled at 10,240 Hz, in order to achieve df = 2.5 Hz, the frame size, N, is set to 4096.

B. Determination of Synchronous Frequency

The synchronous frequency (SF) plays a very important role since cage frequency locations are estimated using SF. Assuming that SF exists, one way to find the SF is to look for the maximum. However, typical cases have shown that the problem is not simplistic. Two problems arose: 1. Due to discretization error, the SF seemed to fluctuate about the expected value, 2. In some cases, SF does not manifest itself for a duration of time due to very high noise level. The two problems mentioned above are illustrated in Figure 4.2.

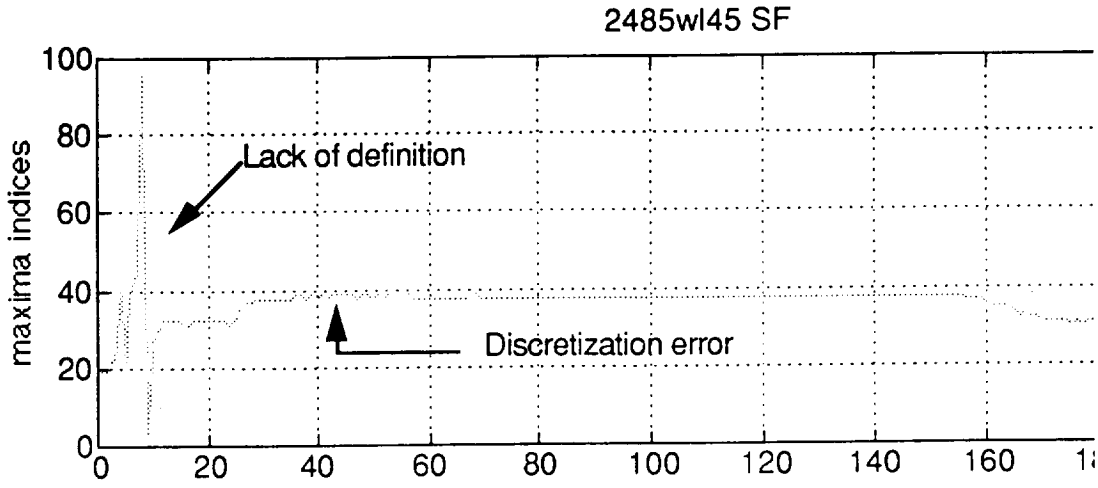

Figure 4.2 Typical Error in Finding Synchronous Frequency

The lack of synchronous response is overcome in other SSME pumps with the use of dedicated speed transducer channels which utilize magenetic pickup type technology. Unfortunately, the SSME HPOTP speed transducer was not included in the engine design due to the high dynamic pressure environments seen at the pump inlet.

Discretization errors, which are often manifested as small transient peaks, can be minimized by using various digital filters, for example, averaging or the Butterworth low pass filter.

For the second case, as shown in Figure 4.2, when the SF is not well defined, further investigation is needed. Figure 4.3 displays the first 20 frames of 2485wl45. The SF is not well established in the first 10 frames, thus creating incorrect maximum indices. One method of dealing with the lack of definition is to ignore the engine data until an obvious SF is found. This method can be used only if it is assured that SF is found for most of the cases. This 'ignore-if-not-sure method' was not considered since loss of information may be too great when SF is not manifested for a significant duration. An alternate set of algorithms are investigated to deal with the ill-defined area. Two such algorithms take into consideration the analysts' apriori knowledge of the SF: Credibility and Correlation.

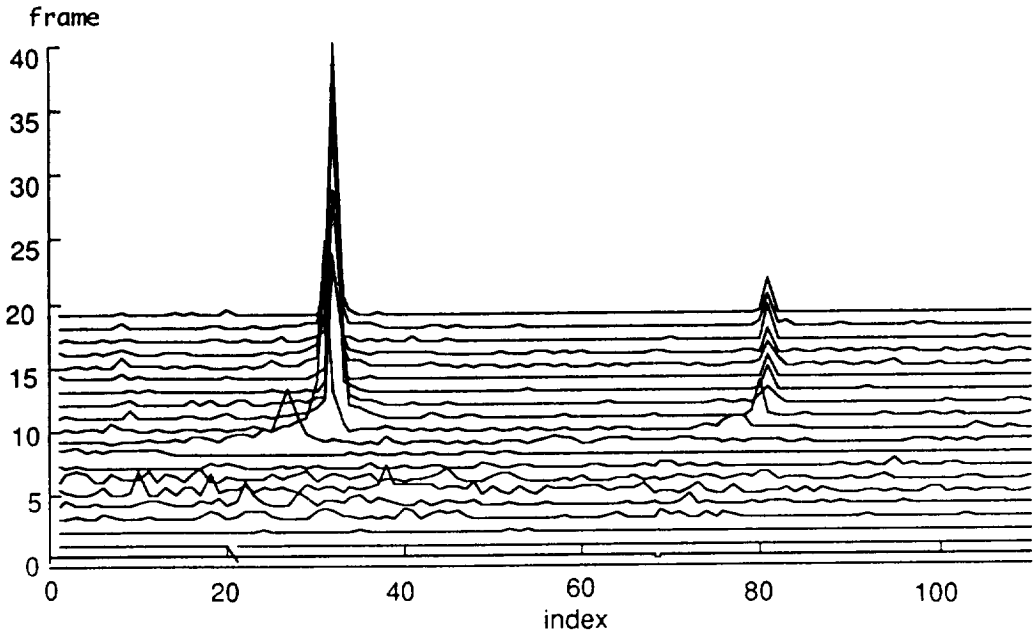

Figure 4.3 Ill-defined Synchronous Frequency(2485wl45)

1. Credibility Filter

The first approach deals with credibility of a data point using a simple credibility filter. A set of credibility filters is constructed based on the analysts' experience. A set of trapezoid filters is generated. The center of the trapezoid filter is defined by a priori knowledge. As a data point falls away from the center, the data point becomes less credible. As the data point gets closer to the mean, the better credibility the data point will have. A series of trapezoid credibility filters were defined as shown in Figure 4.4.

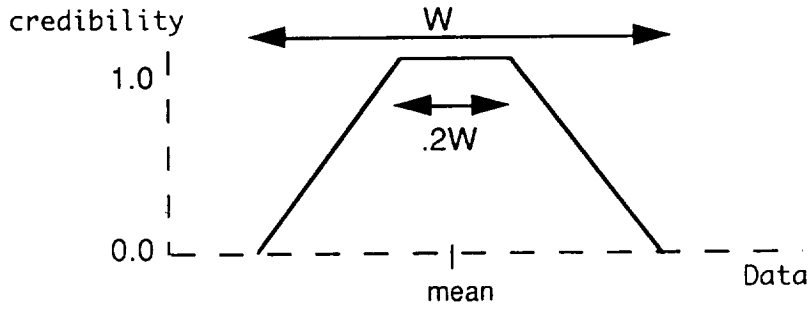

Figure 4.4 Credibility Filter.

The credibility is defined as follows:

$$CR = \begin{cases} 1.0 & \text{if ABS(Mean-data) =< 0.1W} \\ 0.0 & \text{if ABS(Mean-data) > 0.5W} \\ 1-(5/2W)(ABS(Mean-data)-0.1W) & \text{otherwise} \end{cases}$$

where W is the width of the filter,
Mean is the mean of the filter,
ABS is absolute value.

Using a linear model, based on an empirical model, a set of predicted SF is calculated based on the thrust level schedule (Figure 4.5). The predicted SF is used to construct a series of credibility filters as shown in Figure 4.6.

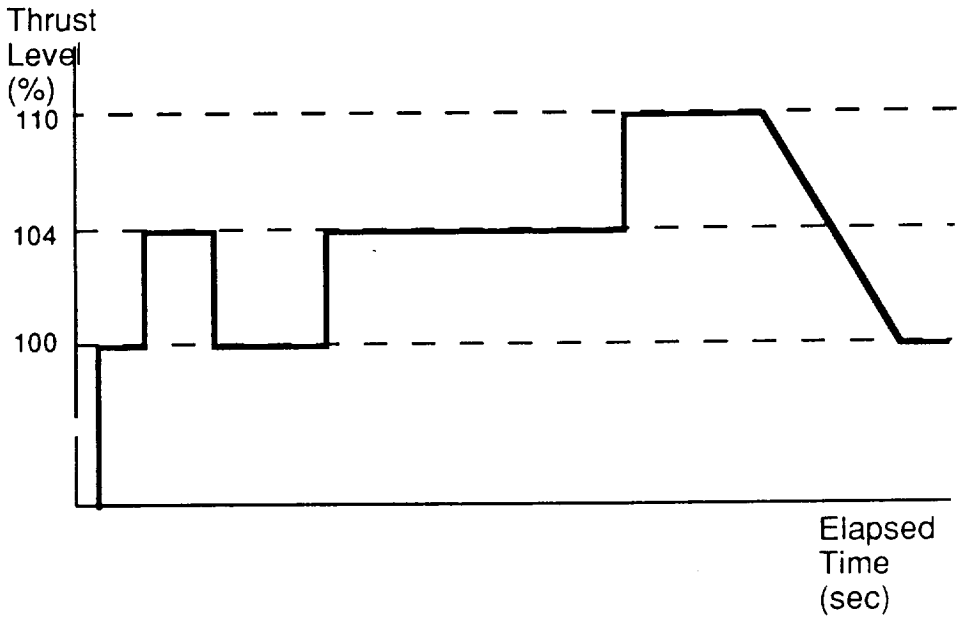

Figure 4.5 Example of Thrust Level Changes

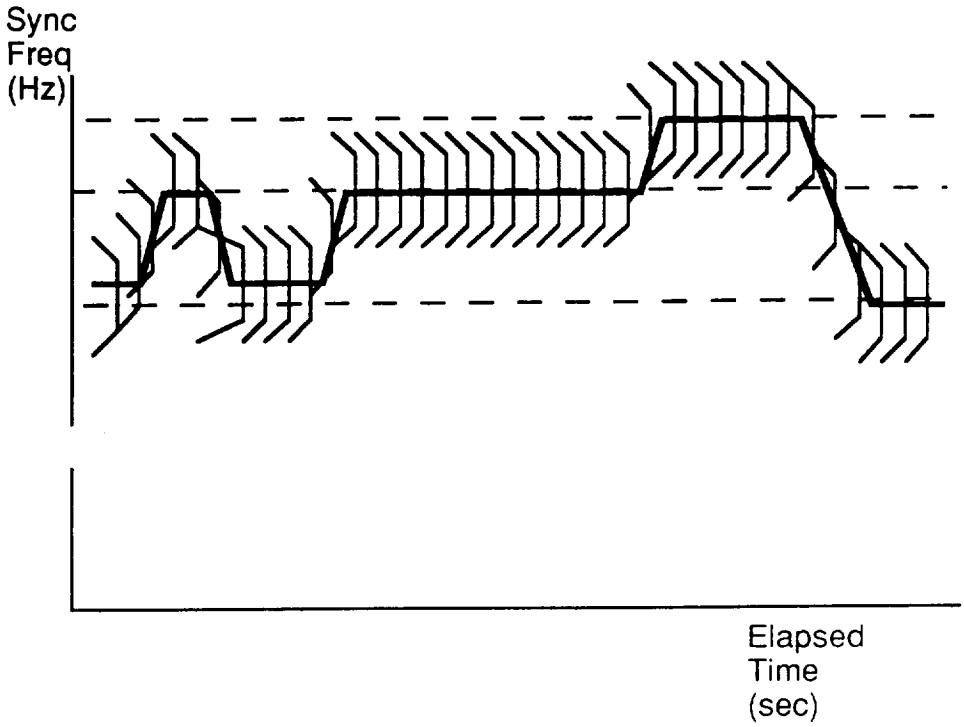

Figure 4.6 Two-dimensional Credibility Filter with Moving Mean

After credibility of each data point is determined, a simple rule is implemented: The less credible a data point is, the more important the a priori information is. As the data point becomes more credible, the less dominant the a priori knowledge is. This rule implementation is illustrated as Figure 4.7.

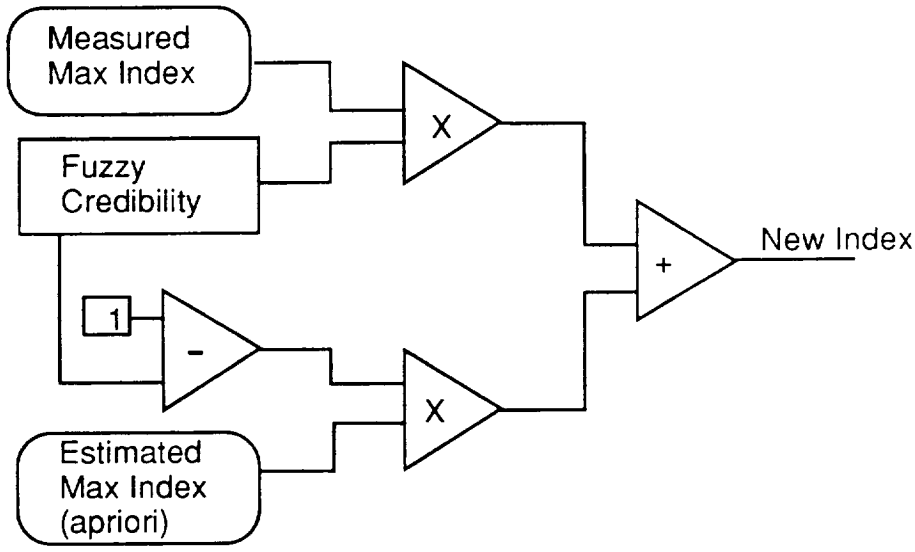

Figure 4.7 Credibility Implementation

Using the credibility filter with W=10, the results are shown as below in Figure 4.8. It seemed that the level of the high pressure fuel turbo pump was as high as the SF such that maxima found fluctuated between the level of SF and the high pressure fuel turbo pump. Figure 4.8 illustrates a case where a credibility filter effectively eliminated erroneous information. Figure 4.8.a is a plot of maxima found. By comparing against the expected SF, a credibility plot is generated as shown in Figure 4.8.c. Finally a new set of SF is found. The absolute value of the difference between the expected values and the processed values is shown in Figure 4.8.e.

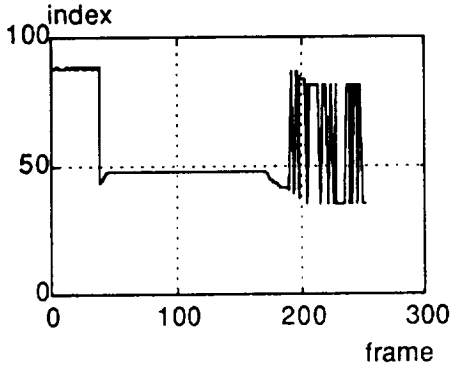

(a) Raw SF (maxima found)

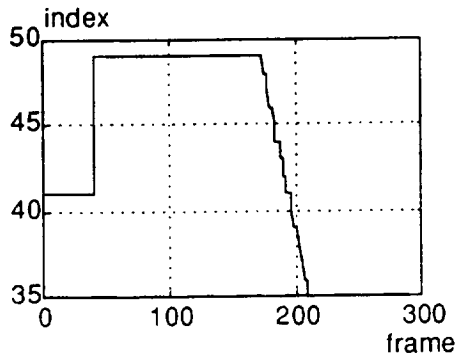

(b)Expected SF

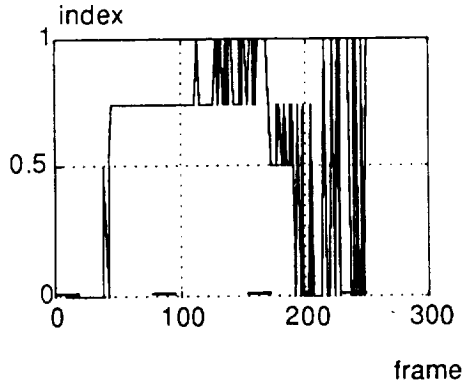

(c) Credibility

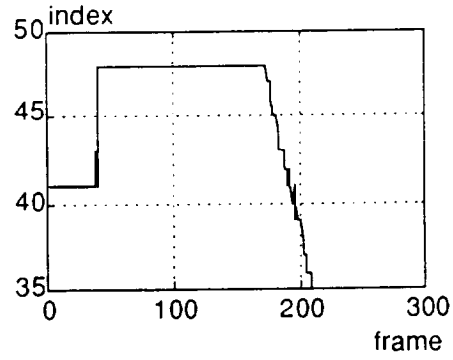

(d) processed SF

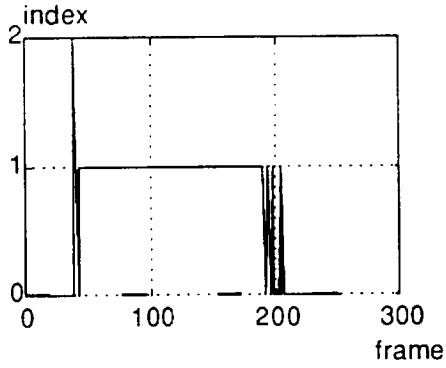

(e) abs(Expected SF - Processed SF)

Figure 4.8 Credibility Filter Results (1595ht135)

Even though the credibility filters were effective for many of the cases, some data files resulted in less than satisfactory results. Two factors contributed to the poor results: One reason was that a linear model deviated significantly from the actual data. It seemed that the linear model used to calculate the center of the trapazoid filter was not accurate. This model error resulted in low credibility, thus causing a large compensation in the SF level, which became another source of error. Another drawback in the credibility filter was its inability to remove discretization error. Discretization error, which is manifested in the form of small transient noise, maps into a credibility value approximately equal to the noiseless signal. In order to minimize this type of erroneous reasoning, more elaborate decision criteria had to be implemented.

2. Correlation

The second approach to find SF considered an overall shape of the expected SF and the found SF. Pearson's r [Weaver, 1983] is used to determine the correlation between the found SF and the expected SF. If linear correlation exists, then a new SF is generated based on the expected SF and the actual data (see Figure 4.9.).

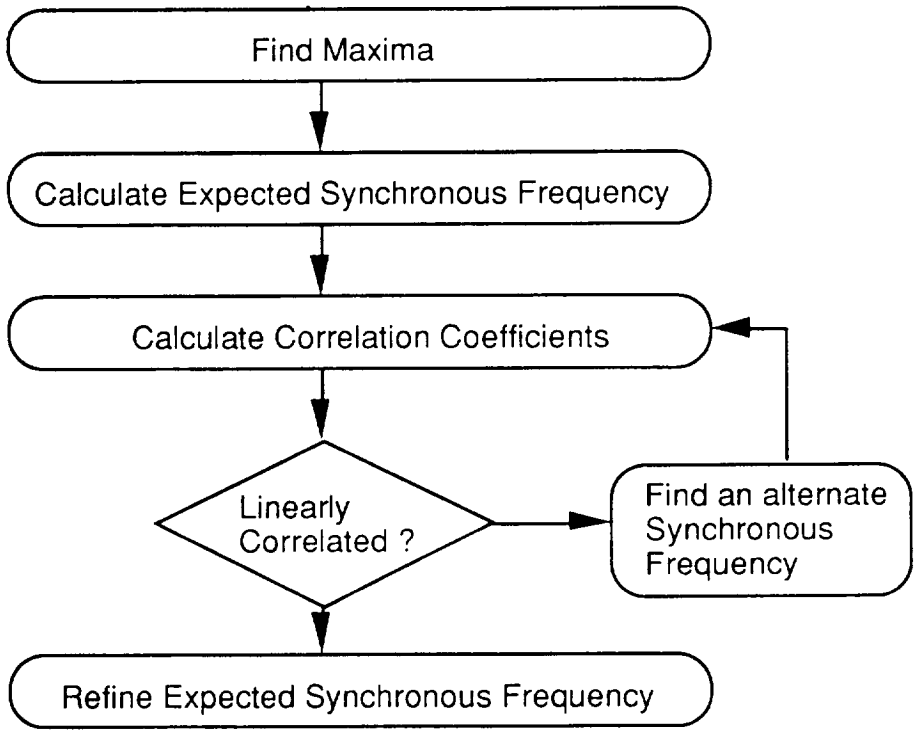

Figure 4.9 Flowchart: Synchronous Frequency using Correlation

By use of Pearson's r coefficient, correlation coefficients of two sets of parameters are found (see Equation 4.2.1). Its linear correlation threshold varies with the sample size. For a set of data pairs, {(x,y)}, whose mean and standard deviations are μ, σ respectively, Pearson's r is defined as :

$$r = \sum_{i=1}^{N} \frac{(\mu_x - x_i)(\mu_y - y_i)}{\sigma_x \sigma_y N} \qquad \text{- - - - (Equation 4.2.1)}$$

[Weaver, 1983]

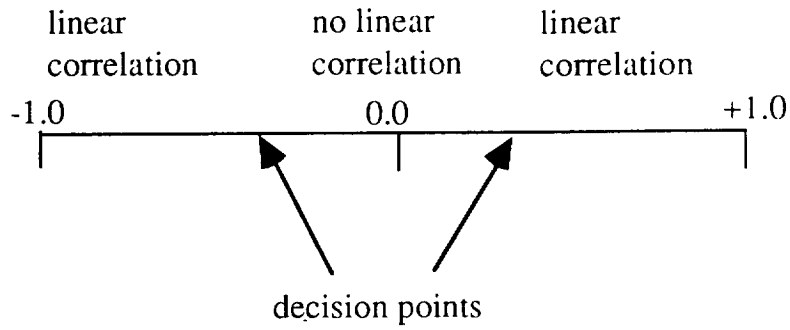

Figure 4.10 Linear Correlation Regions

Decision points are given in absolute values, and the value is inversely related to the size of samples. An example is given in Table 4.1 (Weaver, 1983). For example, with the sample size of 100, the decision points are +/- 0.196 with 95% confidence [Pearson, Hartley, 1966].

SampleSize	DecisionPt	SampleSize	DecisionPt	SampleSize	DecisionPt
5	0.878	20	0.444	80	0.220
10	0.632	50	0.279	100	0.196

Table 4.1 A Guide to Use Pearson's r Coefficient [Weaver, 1983]

An algorithm to use the correlation coefficients is described as follows:

1. Find the potential SF by using the maxima function.

2. Compare the found SF against the thrust level schedule.

3. If the found SF and expected SF are linearly correlated, then find a multiplication factor using Equation 4.2.2.

$$k = \frac{1}{N}\sum_{i=1}^{N}\frac{L_{f(i)}}{L_{e(i)}} \qquad \text{(Equation 4.2.2)}$$

where $L_{f(i)}$ is the ith thrust level found, and $L_{e(i)}$ is the ith expected thrust level. The multiplication factor, k, is an average of ratios of expected and found values during constant power thrust levels.

If they are not linearly correlated, use alternate methods, such as credibilility filters to find another candidate. Continue until a suitable candidate is found.

4. Multiply k by the expected thrust level to acquire a new SF.

This method is simple to implement and proved to be less noisy than the credibility method. The correlation / linearization method seemed to create clean peaks on the 3-D plot. A typical example is shown in Figure 4.11.

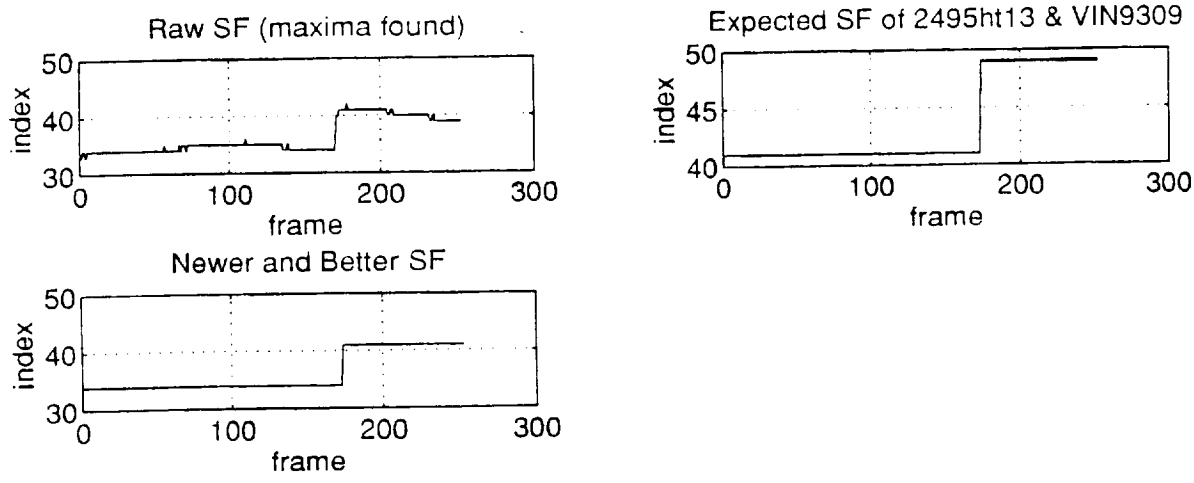

Figure 4.11 Correlation Coefficients Results
(2495ht135)

3. Cage Frequencies

The approximate location of the second harmonic cage frequency, 2C, is found by multiplying the Synchronous Frequency by a factor of 0.86 (= 2x0.43) which is found based on bearing symmetry. In most cases, up to 7C can be investigated. For simplicity, 2C and 3C are included in each file for testing. Since the Synchronous Frequency is determined in terms of indices as described in Section 2, Chapter 4, cage frequencies are derived in terms of indices as follows:

Definition:

SFi as the index of SF,
2Ci as the index of 2C,
3Ci as the index of 3C,
StF as the start frequency of a data file in Hz,
SF as the Synchronous Frequency in Hz,
df as the frequency resolution in Hz,
2C, 3C as the two times and three times the cage frequencies respectively in Hz.
The first index is 1.

Frequency index, Fi, can be expressed in terms of frequency, F, and StF,

$F = (Fi - 1) \times df + StF$ ..... (1)

By definition,

$2C = 2 \times 0.43 \times SF$

substituting in SF in place of F using (1),

$= 0.86 \times ((SFi - 1) \times df + StF)$ ..... (2)

Then $2Ci = (2C - StF)/df + 1$

substituting in equation (2),

$= 1/df \times (0.86((SFi-1) \times df + StF) - StF) + 1$

$= 0.86SFi - (1-0.86)/df \times StF - 0.86 + 1$

$= 0.86SFi - 0.14/df \times StF + 0.14$ ..... (3)

By the same method,

$$3Ci = 3 \times 0.43 \times SF \text{ reduces to}$$
$$= 1.29 \times SFi + 0.29/df \times StF - 1.29 + 1 \ldots\ldots (4)$$

Actual values of 2Ci and 3Ci are the closest integers to the calculated values. For example, if a file starts at 375 Hz, where the index is 1, and SFi is determined to be 35 (or 460 Hz) with a frequency resolution of 2.5 Hz, then

$2Ci = 9$ (or 395 Hz),

$3Ci = 89$ (or 595 Hz).

Using equations (3) and (4), locations of the expected 2C and 3C are found as shown in Figure 4.10.

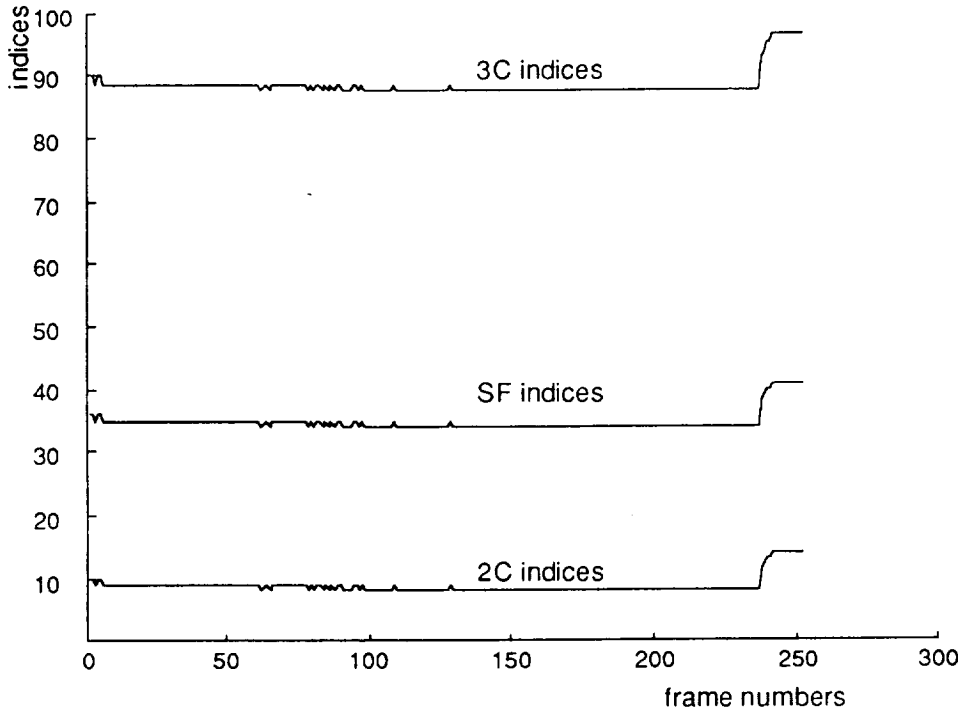

Figure 4.10 446HT45 SF, and expected 2C/3C indices
(Raw data without filtering)

D. Anomaly Detection

1. ANN Approach

To detect anomalous peaks, Artificial Neural Networks (ANN) are developed. Various configurations are considered to optimize the design. Several tests using various ANN configurations were performed to find an optimal configuration. Most of the tested cases used a frequency resolution of 2.5 Hz since this frequency resolution value is most often used by analysts. One case used 1.25 Hz case. For the neural network training, MatLab (MathWorks, Inc.) and NETS (NASA Johnson Space Center) were used. Both of these software tools utilize the back-propagation algorithm for training.

a. Initial Training and Propagation Results

The input to the ANN consisted of thirteen points centered about the expected cage frequency. To generate a training set for the neural networks, two approaches were considered. The first approach was to make a manual decision on each individual frame of a data file. This approach was done by manually examining each frame of data to see if an obvious anomaly existed. Understandably, this approach required considerable manpower and patience to generate a sufficiently large training set. This approach involved manually labeling normal and abnormal frames. First of all, an anomalous data file, 2485PB45, was chosen. The file was normalized between 0 and 1, and a decision was manually made by a human operator on each frame. Decision assignment was 0.9 for nominal, and 0.1 for anomalous frames. This task was quite subjective, and at times proved to be very difficult to determine its assignment. There were many cases where the decision of anomalous/nominal was very difficult. However, it was assumed that if 'enough good information' is given to the neural network, the network should be able to learn the desired patterns. A total of two hundred and seven frames were individually evaluated and tagged. Seven artificial sets were added to accentuate the importance of the middle of the frame. Over all, the training file included 149 anomalous frames and 58 nominal frames. The neural network consisted of 13 input neurons, 8

hidden layer neurons, and 1 output neuron. After several iterations, RMS error was reduced to 0.11, and the training was halted. The training set was used to verify the learning. The results were almost inconceivable. Out of 207 frames, there were only 2 errors. This accurate mapping seemed surprisingly good due to the subjective nature of the manual decisions. However, good training did not seem to translate to a better design. When tested using other files, this network failed. It seems that the network has learned some specific idiosyncrasies about the training set, and the learned behavior was not able to generalize. This conclusion was verified further by re-examining the training file. One of the artificial frames was mistakenly labelled wrong, and the neural network mapped this frame just as it was trained. This ability to converge to the training set was impressive, but the lack of generalization was of serious concern. More tests will be required to characterize this behavior using larger sets of training data.

The second approach was selecting one data file with nominal data and another data file containing anomalies. Then each file is tagged as normal (0.9) and abnormal (0.1). The objective of this approach was to see if the ANN could learn by itself the inherent distinction between normal and abnormal cases. This approach to label each data file as a whole must contain 'enough good information.' On many occasions, the cage frequencies do not appear for the full duration of the test. Therefore, a subjective decision should be made whether a file include enough good information.

Due to their inherent properties, ANNs do not lend themselves to thorough verification. However, it is necessary to have some understanding of the trained network. A file, 2474wld0, was used to propagate and to test the trained network using the file labeling. The file included 13 points centered at the calculated cage frequencies (2C and 3C). The 13 points were normalized such that the lowest value was set to 0, the highest 1. When the data was propagated, the results seemed to be inaccurate. Defining the correct response to be less than 0.2, out of 250 frames, the ANN found 3 hits for 2C case, and 10 hits for 3C. It was hypothesized that the reason for the low hits was due to the skewing of the peaks. Each data set was shifted left one at a time, and 0.5 was added as the 13th element. The following results were compiled with shifting.

	2C	3C
shift left 0	3	10
shift left 1	3	28
shift left 2	34	15
shift left 3	4	N/A

Table 4.2 Network Testing with Shifts

It became apparent that the trained network was very sensitive about the position of the peaks.. Using this information, an ANN architecture was implemented to use rotated input sequences.

b. Artificial Neural Network Design

i. Rotate and Propagate

An artificial neural network with 13 input neurons, 8 hidden layer neurons, and 1 output neuron was trained with two 2.5 Hz files: 446ht13L (anomalous) and 2495ht13L (nominal). These two files are generated using the Pearson's r and linearization technique as described in Section B.2, Chapter IV. Then 3C file from 446ht13 was used for consistent peaks (see Figure 4.13).

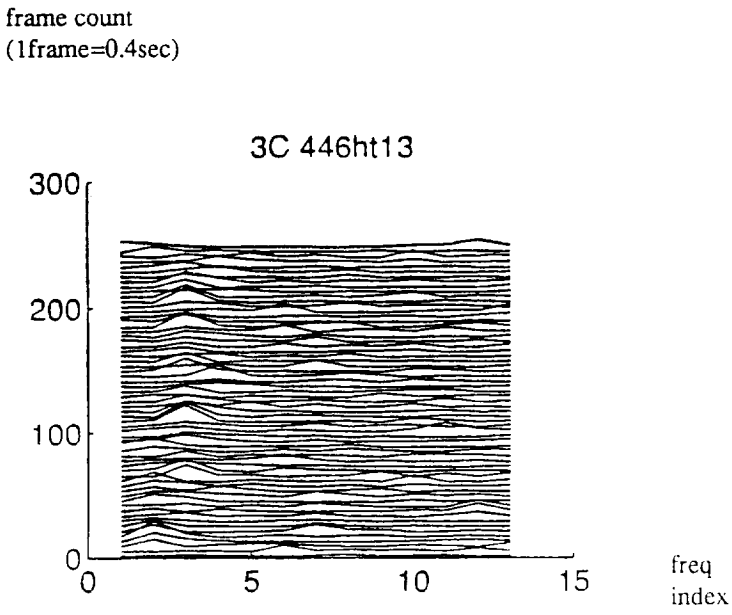

Figure 4.13 446ht13L file (anomalous) for training

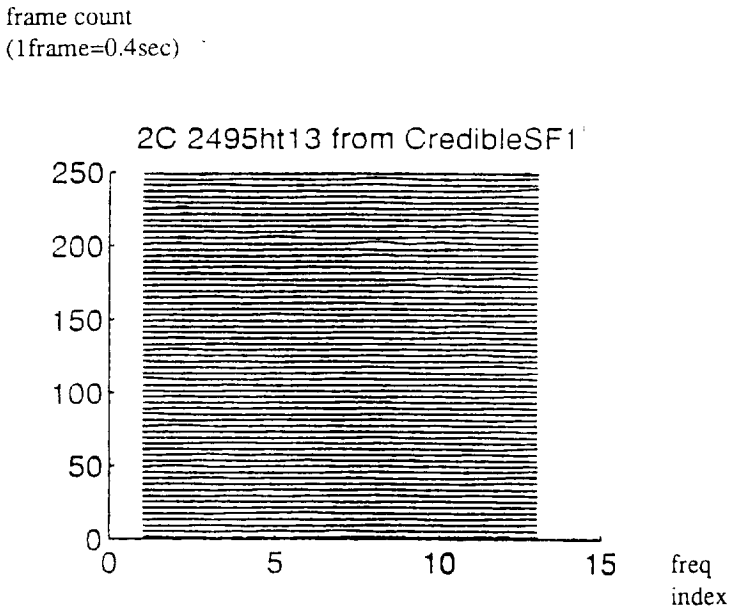

Figure 4.14 2495ht13L file (nominal) for training

To reveal the nature of the training sets, maxima location of each frame was determined and plotted (Figures 4.15 and 4.16). The nominal training set (2495ht13L) displays even distribution of maxima whereas the anomalous case (figure 4.16) has over 70% of its maxima located in the frequency bin #3. This contrast in peak distribution is used to train neural networks.

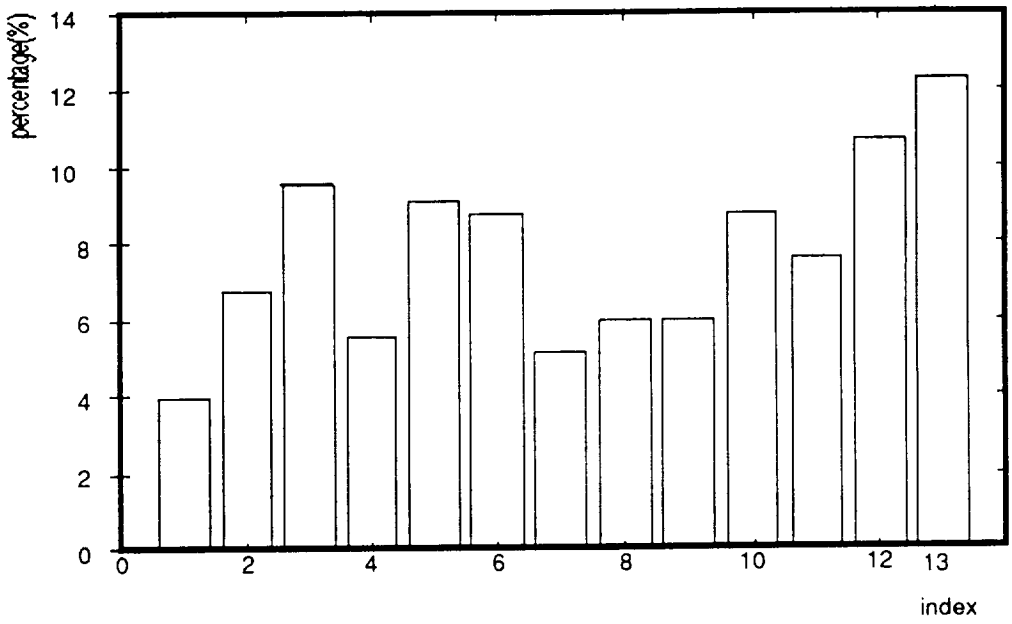

Figure 4.15 Maxima Distribution of 2495ht13L(Nominal)

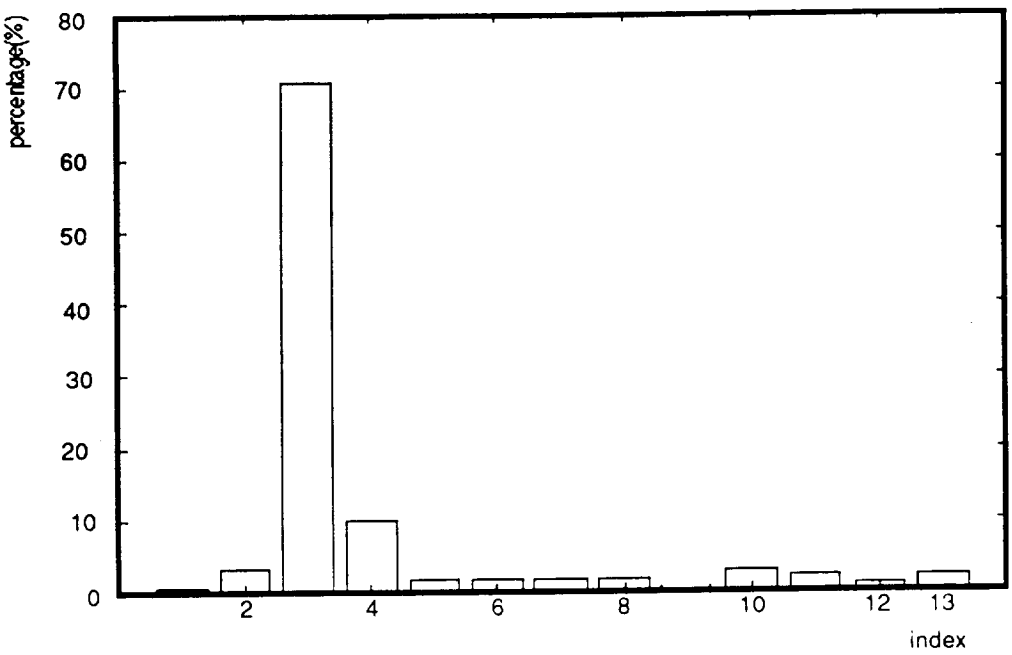

Figure 4.16. Maxima Distribution of 446t13L (Anomalous)

The training was done using back propagation with various learning rates. The output assignments were 0.1 for the nominal case, and 0.9 for the anomalous case. The first training set consisted of the above two files appended consecutively. Each file contained 252 time frames with normalized magnitude to have the maximum magnitude of 1 and minimum of 0. Training a neural network involves fairly mundane tasks of selecting transfer functions, hidden layers, transfer functions, etc. Various learning rates were used ranging from 1 to 0.001. High learning rates seemed to incur rapid changes, usually resulting in oscillation, but overall error did not seem to get smaller. It seemed that a learning rate of 0.01 allowed a reasonable training point. The transfer function used for this training was the Logsig function (see Figure 4.17).

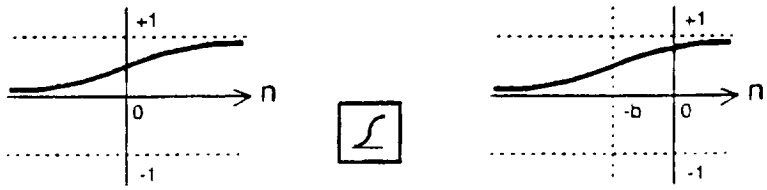

Figure 4.17 Logsig Transfer function

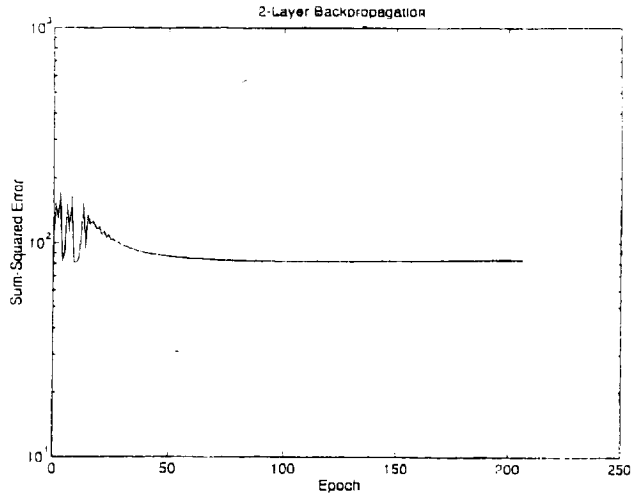

Figure 4.18 Learning Rate = 1

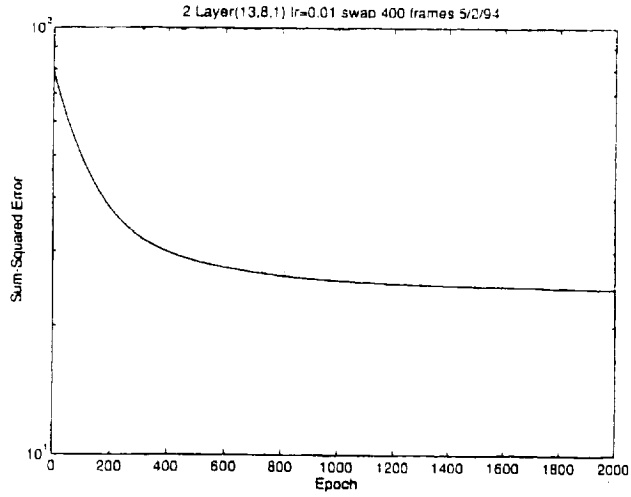

Figure 4.19 Learing Rate = 0.01

One aspect of the learning was of concern. If the neural network was presented with 252 of the anomalous frames first, would the network prematurely converge before nominal data can be presented? Would a mixed training set perform better? With these questions in mind, 400 frames out of 504 frames were randomly selected and swapped. Using the same learning rate of 0.01, a new learning was performed. There was a faster reduction of summed squared error using the randomly swapped input file (Figure 4.21). And at 1000 epochs, the error was reduced to approximately 250, as opposed to over 300 for the non-swapped case. After 2000 epochs the training stopped (See **Appendix A** for the weights and biases).

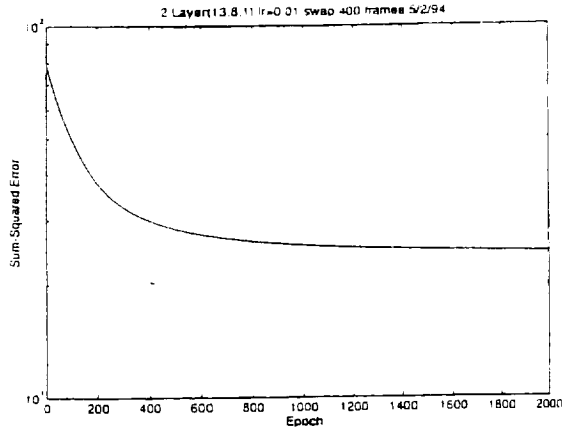

Figure 4.20 Sequential Training

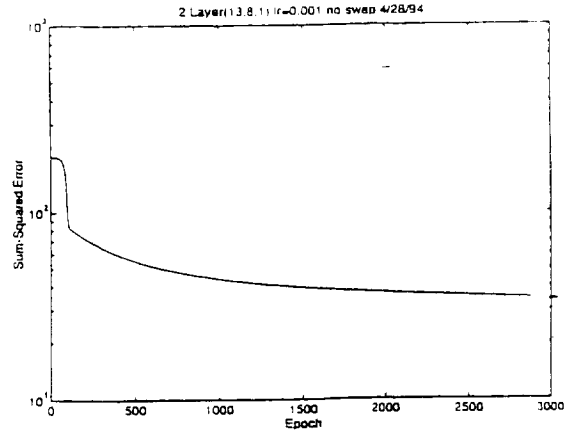

Figure 4.21 Alternate Training

A hit is defined to be a propagated value greater than or equal to 8.5 and less than 9.5. Initial propagations indicated that the network was very sensitive to the magnitude and location of the peaks. For example, when raw data is propagated without normalization, there were 0 hits. Also when the peaks were shifted, the results were less than satisfactory. Using these observations, all data sets were scaled such that the maximum number in the file would be 1.0. In addition, the 13 data points were rotated and propagated to find consistent peaks(Figure 4.22). The results are summarized in the Table 4.3.

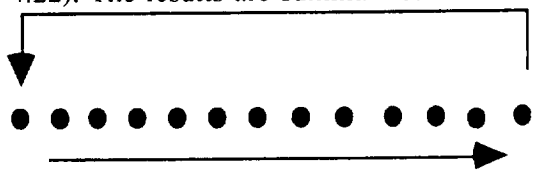

Figure 4.22 Rotate and Propagate

File Name	ANN 2C Hits	ANN 3C Hits	ANN Decision	*Experts Decision
1595PB45	21	37		
1595WL45	20	50	max=21,50	2
1675HT135	17	13		
1675PB45	5	21		
1675WL45	34	34	max=34, 34	2
2495HT135L :Training Set	14	148		
2495PB45	11	105		
2495WL45	19	164	max=19,168	0
446HT135 :Training Set	14	123		
446PB45	19	29		
446WL45	11	92		
446WLD0	26	17	max=26,123	3

Note *: Expert's decision is denoted 0 to 5, where 0 represents normal data and 5 represents highly recognizable anomaly.

Table 4.3 Rotate and Propagate

Inspection of the results, as shown in Table 4.3, seems to indicate correlation between the peaks and the hits. A high number of hits represents a consistent series of peaks. What did the neural network learn? Did the network understand the concept of anomalous peaks? To understand the inner workings of the neural networks, a test is performed with a known parameter that assimilates anomalous peaks. It is shown from previous cases that maximum values seem to represent the prominent peaks, as shown in figures 4.15 and 4.16. Thus a test is performed to see if the locations of maxima are correlated with the neural network output. Even though the 2495wl45L file does not include any anomalous peaks, the file includes consistent peaks (high pressure fuel synchronous feedthrough) that can be used as test peaks for the neural network. It is evident from the plots (Figure 4.23), the trained network correctly identifies maximum peaks located at the frequency bin #3 (Figure 4.23.i). When the peaks are shifted right 1 time such that the peaks are now located in the bin #4, the neural network is able to detect the peaks with some noise. However, when the peaks are shifted left, the network is not able to detect the peaks at all. Since the maxima seem to be at two discrete levels for this case, two ANN output readings can be made for each index for better understanding of peak locations and ANN outputs. Table 4.4 delineates the statistical distribution of the ANN output. 'Index' column represents an index where maximum values fall. For example, after 6 shifts (Figure 4.23.g), the majority of maxima fall in index 1 and index 12. Mean and standard deviation is calculated for these two indices and tabulated. This process is continued until all data has been tabulated. Inspection of the table seems to indicate close correlation of the maxima location and the neural network output.

Another observation is made about the neural network. When the maxima is located at index #4, the neural network produced high output signaling peak detection. This may be due to an unintended source of error in the training data set. The training set 446ht13L included 70% of maxima at index 3 and 10% of maxima at index 4. It seems that the neural network has learned to recognize peaks at location 3 as well as 4. The next four prominent indices (2,10,11,13) in 446ht13L do not seem to affect the output, which is a desirable noise immunity attribute of neural networks.

index	shift	mean	std dv	shift	mean	std dv
1	6	0.0340	0.0091	8	0.0490	0.0183
2	7	0.0310	0.0373	9	0.0425	0.0421
3	8	0.9427	0.0081	10	0.9246	0.0247.
4	9	0.9120	0.0667	11	0.8481	0.0279
5	10	0.0464	0.0192	12	0.0710	0.0340
6	11	0.0881	0.0279	0	0.1206	0.0424
7	12	0.1211	0.0538	1	0.1767	0.0748
8	0	0.5665	0.1082	2	0.4753	0.1030
9	1	0.1080	0.0364	3	0.1377	0.0420
10	2	0.0418	0.0194	4	0.0638	0.0283
11	3	0.3577	0.1002	5	0.3303	0.0998
12	4	0.0465	0.0185	6	0.0682	0.0272
13	5	0.2753	0.0839	7	0.2633	0.0840

Table 4.4 Maxima Location and ANN Output

Figure 4.23 Comparison of Maxima and ANN Output

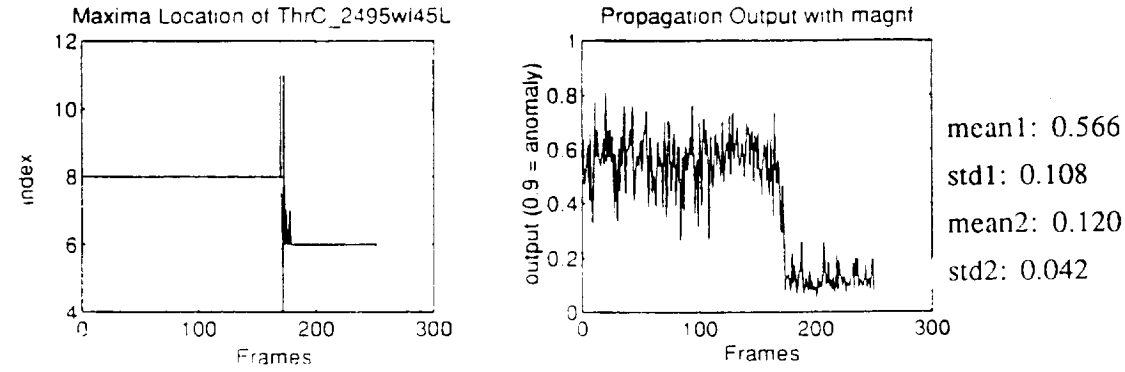

(a) without shift

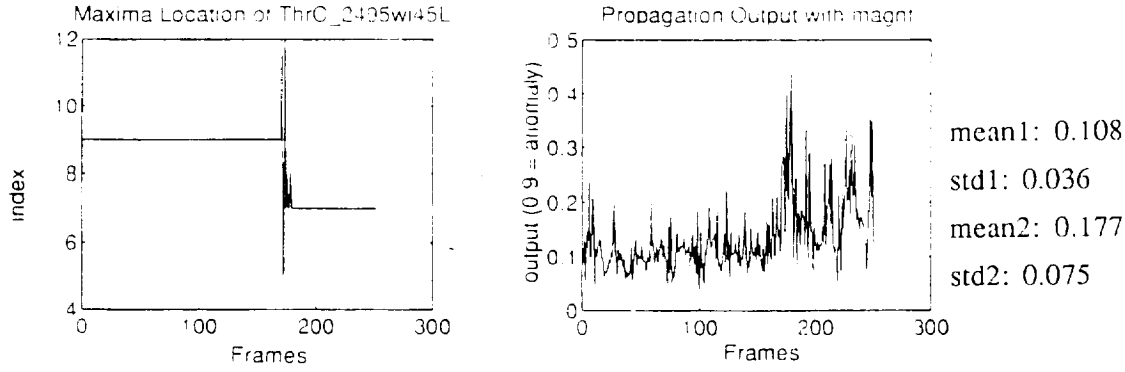

(b) after 1 shift

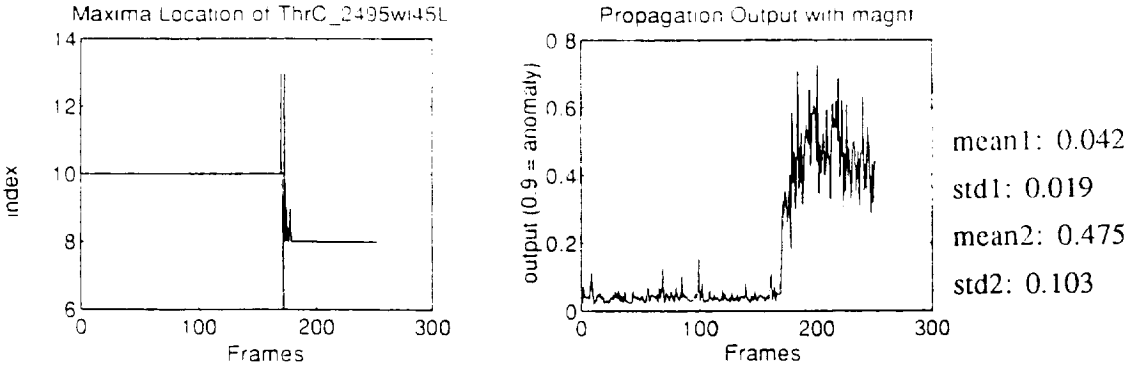

(c) after 2 shifts

Comparison of Maxima and ANN Output(Cont'd)

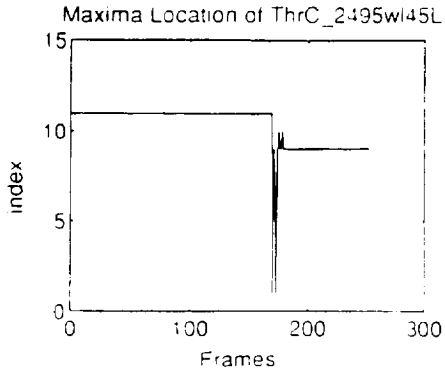

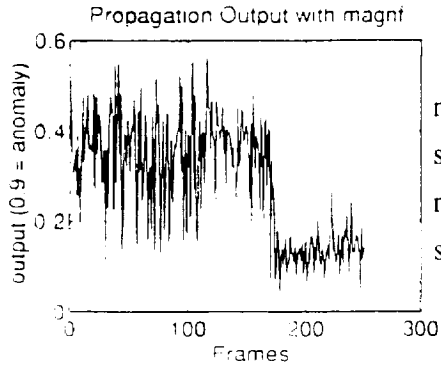

mean1:0.358
std1: 0.100
mean2: 0.138
std2: 0.042

(d) after 3 shifts

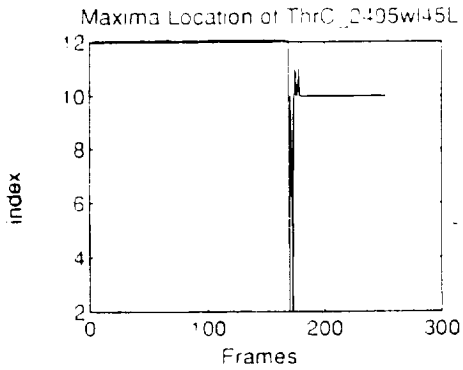

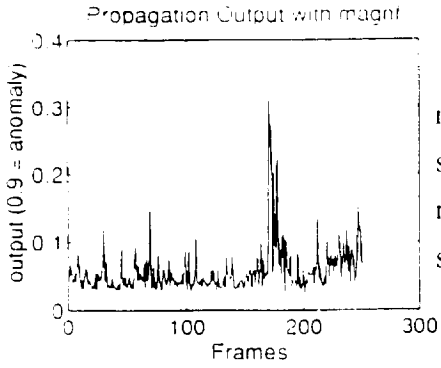

mean1: 0.046
std1: 0.018
mean2: 0.064
std2: 0.028

(e) after 4 shifts

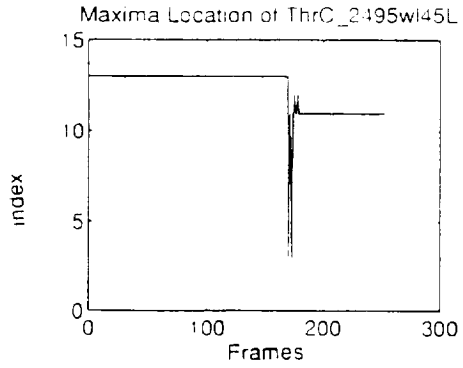

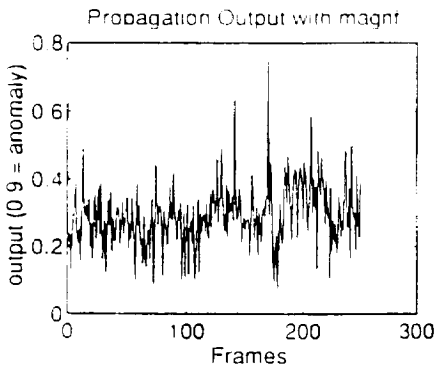

mean1: 0.275
std1: 0.084
mean2: 0.330
std2: 0.100

(f) after 5 shifts

Comparison of Maxima and ANN Output (cont'd)

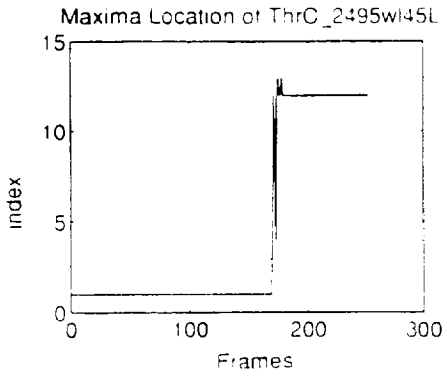

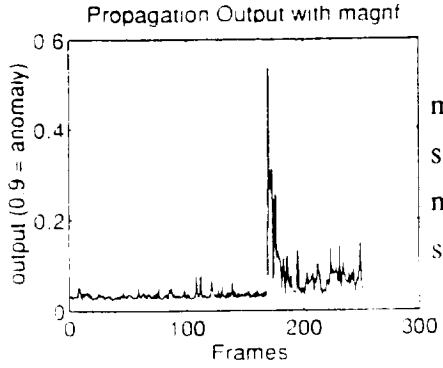

mean1: 0.034
std1: 0.009
mean2: 0.068
std2: 0.027

(g) after 6 shifts

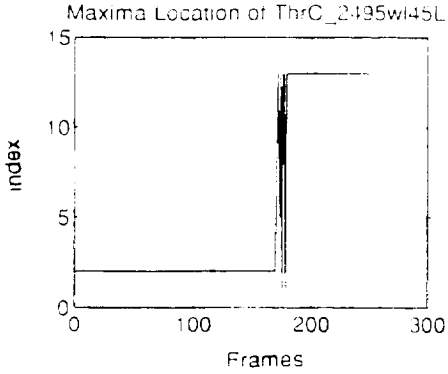

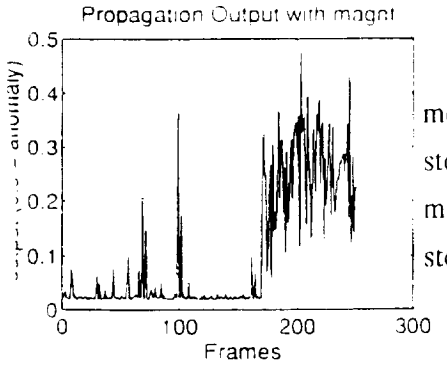

mean1: 0.031
std1: 0.037
mean2: 0.263
std2: 0.084

(h) after 7 shifts

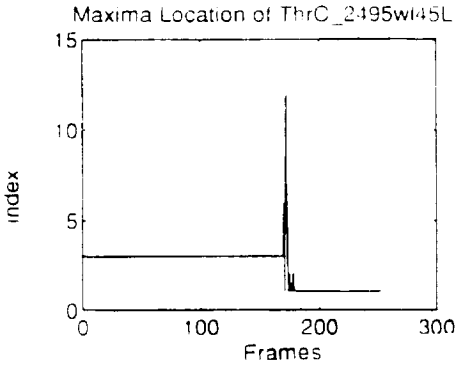

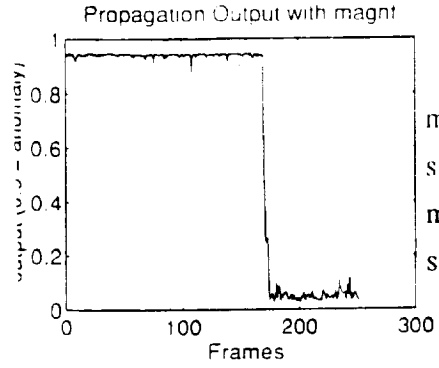

mean1: 0.943
std1: 0.008
mean2: 0.049
std2: 0.018

(i) after 8 shifts

Comparison of Maxima and ANN Output (cont'd)

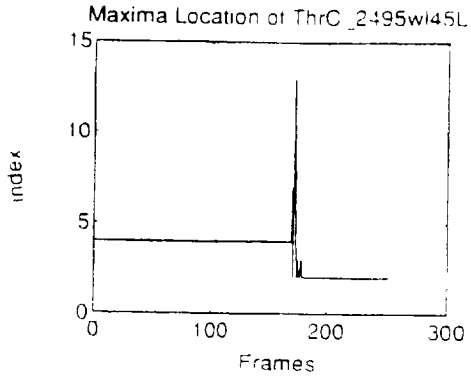

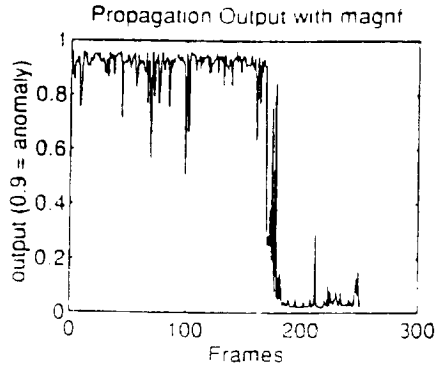

mean1: 0.912
std1: 0.042
mean2: 0.067
std2: 0.042

(j) after 9 shifts

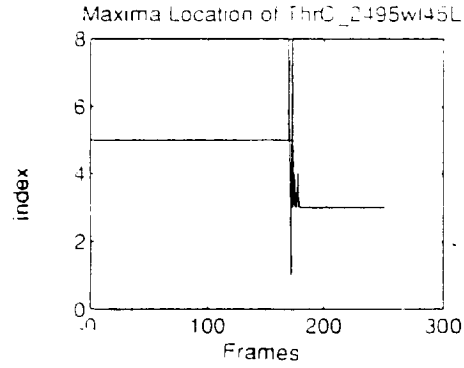

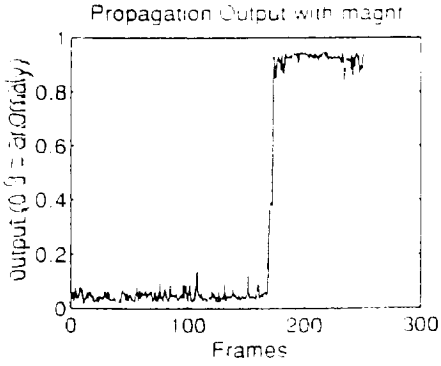

mean1: 0.046
std1: 0.019
mean2: 0.924
std2: 0.025

(k) after 10 shifts

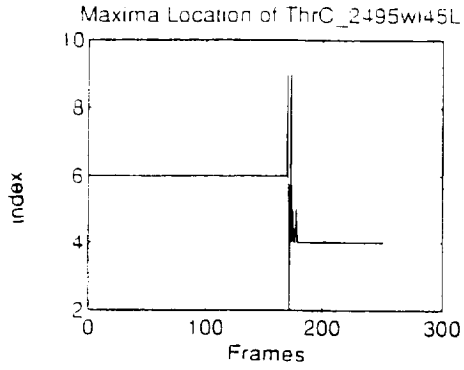

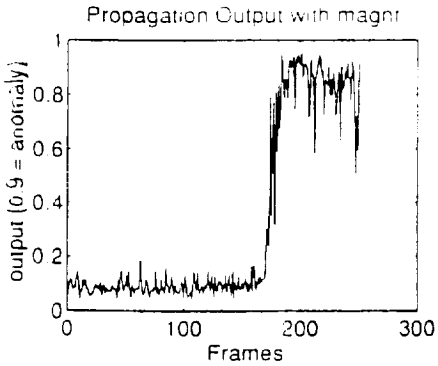

mean1: 0.088
std1: 0.028
mean2: 0.848
std2: 0.097

(l) after 11 shifts

Comparison of Maxima and ANN Output (cont'd)

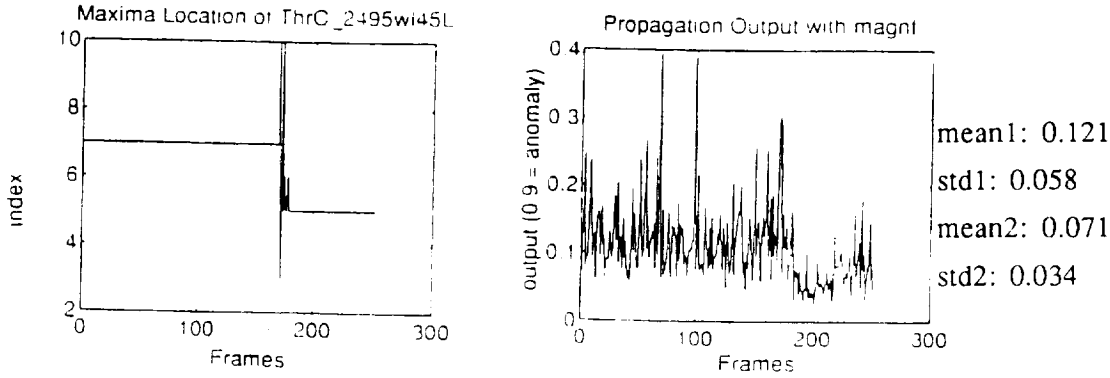

(m) after 12 shifts

b. Other neural network designs

Two other configurations are designed and tested: 1. Shift-and-propagate, 2. Peak Detector. In this document a brief summary is provided for completeness. For further details, refer to Kim and Kissel [Kim, Kissel, 1994].

Shift and Propagate : A network with 13 input nodes with varying size of a hidden layer is trained with two 1.25 Hz files: 2485wl45 (anomalous), and 2495wl45(nominal). For testing, 21 normalized points were selected from each spectral frame centered at the expected frequency. The first 13 points were entered into the trained network for propagation. Then the 21-point data set is shifted left, and 13 points are again input to the trained network. This continues until the last 13 points of the set are used for propagation (Figure 4.24). The trained network performed well to detect 2C peaks.

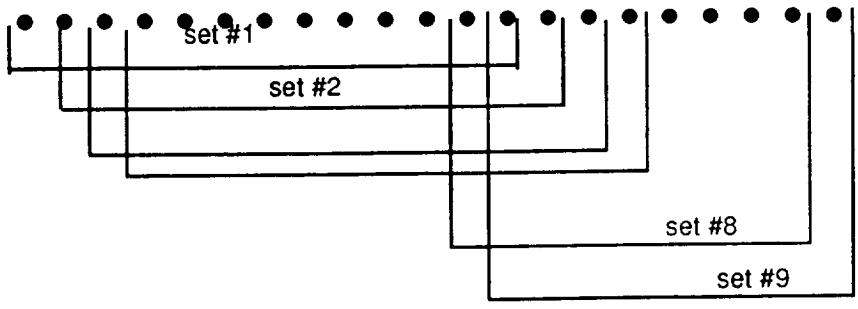

Figure 4.24 Shifted Input Data Sets

Peak Detector : This peak detector design utilizes an assumption that a definition of 'peak' can be taught to the artificial neural network. In order to achieve this learning, two files, 2485wl45 and 2495wl45, were used. Instead of providing 13 points, the peak detector network was provided with 10 frames of 3 points from the two files. If there was an anomaly, the peak would appear consistently at the second (or middle) point of each frame (Figure 4.25). In addition to the purely geometric definition of peak, by providing 10 frames of data, the neural net was to learn about subtleties of any temporal relationship between frames.

Figure 4.25 Peak Detection using 10 Frames

The results using the peak detector seemed accurate. This technique provided not only the number of peaks but the location of the peaks. For more details, refer to Kim and Kissel [Kim, Kissel, 1994].

2. Decision

Until this point, peaks are found using artifical neural networks after performing data reduction using Pearson's r or analog logic. The next task is to establish a statistical data base to determine the threshold such that a decision can be made on the health of SSME turbo pump bearings. One approach can be a pure peak counter as described above. This approach would require a tremendous amount of data and time to establish a numerical threshold value. A better approach is to take into account consecutiveness of peaks. For example, if three peaks appeared consecutively, how much more meaningful is that data instead of seeing three peaks that are scattered? Incidentally, engine analysts employ a similar approach. A series of concentrated peaks are given more significance than the same number of peaks that are randomly distributed.

Table 4.5 delineates the results of peak counting and consecutive peak algorithms. The consecutive peak counting algorithm provides an alternative to examining the anomalous peaks. However, it is not clear from the limited test cases which algorithm is more effective at this time.

File Name	ANN 2C Hits	ANN 3C Hits	2C max conse hits	3C max conse hits	*Expert's Decision
1595PB45	21	37	2	11	
1595WL45	20	50	2	11	2
1675HT135	17	13	1	1	
1675PB45	5	21	2	1	
1675WL45	34	34	3	2	2
2495HT135L :Training Set	14	148	1	23	
2495PB45	11	105	1	9	
2495WL45	19	164	1	164	0
446HT135 :Training Set	14	123	2	9	
446PB45	19	29	1	2	
446WL45	11	92	1	3	
446WLD0	26	17	1	5	3

Note *: Expert's decision is denoted 0 to 5, where 0 represents normal data, and 5 represents highly recognizable anomaly.

Table 4.5 Results of Peak Counting and Consecutive Peak Algorithm

Chapter V

CONCLUSIONS

A definition of knowledge was proposed in this document to provide a framework to model human knowledge. Knowledge classification was defined as Explicitly Accessible, Implicitly Accessible, and Inaccessible. Analog logic and ANNs were effectively used to model a decision process to detect anomalous cage frequencies.

The Space Shuttle Main Engine (SSME) High Pressure Oxygen Turbopump (HPOTP) data, sampled at 10,240 Hz from various external locations using strain guages and accelerometers, were converted to frequency domain data using the Fast Fourier Transform. In order to reduce the data, analog logic and correlation were implemented to extract the areas of interest. Credibility filters and Pearson's r were implemented to construct the Synchronous Frequency from which cage frequency locations were estimated. This approach was implemented to produce thirteen points centered about the expected cage harmonic frequency location.

ANNs were trained using the back propagation technique to determine peaks in the spectral domain. Several configurations of artificial neural networks were tested and documented. The ANNs seemed to identify peaks correctly to assimilate human analysts' visual inspection. A statistical distribution of maxima was compared with the results from ANN propagation to gain insight into the trained network. This statistical distribution seemed to indicate that the location of the maxima had a strong correlation with the output of the neural network. The neural network seemed to have learned its mapping of input and output without explicit instructions.

There are many features that make this type of approach suitable for automation of manual tasks. Definition of knowledge and modeling techniques allows easier translation of human knowledge to computerized automation. Analog logic allows direct translation of linguistic expression to quantitative numbers. ANNs can be implemented to optimize their self-learning capabilities without explicit instructions. ANNs can be especially beneficial when human knowledge is difficult to articulate.

Based on this research, the following tasks are proposed to be investigated further:

- In order to make an automated system, a more advanced type of decision algorithm is required to take into account the intensity of the peaks, discrimination of line noise from abnormal data, and past experiences.
- Better definition of 60Hz data and other pertinent information, such as fuel pump data, should be given to the neural networks so that cage frequency can be discriminated from other irrelevant data.

Appendix A:

Artificial Neural Network Parameters

SHIFT AND PROPAGATE PARAMETERS (1 of 2)

W1 =

Columns 1 through 7

-0.2205	0.0255	-0.0294	-0.3790	0.1606	0.2493	-0.2605
1.4083	-1.7710	-0.8315	0.2501	1.6040	0.9984	-0.5730
-0.4572	0.3848	0.4565	0.1258	0.3068	0.1800	0.0555
0.7994	-0.1463	0.1157	1.0177	-1.1560	0.1994	1.6783
-0.8600	-0.6219	-1.2588	-0.5633	-1.2257	-0.1862	-0.8889
-0.4106	0.1560	0.0750	-0.4506	0.1744	-0.2894	-0.1357
0.2012	0.0906	-0.4790	0.0437	-0.9882	0.0499	0.4524
-0.7805	-0.1112	0.0090	-1.3214	0.1259	1.4597	-0.6140
0.5324	-0.3947	0.5893	-0.4454	1.4631	0.6267	1.6365

Columns 8 through 14

-0.0277	-0.3377	-0.5169	0.0042	-0.1252	-0.3800	-0.2069
-1.4170	0.2880	-0.8322	-0.9631	0.6908	0.7943	-0.4423
-0.1385	0.7119	0.0442	-0.2153	0.6068	0.0852	-0.0662
-0.3966	0.2238	1.4413	-0.1822	1.1730	0.7878	-1.3708
-0.9446	0.3958	-0.6383	-0.9919	1.4657	-0.2012	-0.5888
0.0522	0.0559	-0.6805	0.2698	0.0850	-0.1366	0.1491
-1.0306	-0.0861	-0.0553	-0.0379	-0.0984	-0.6341	-0.7628
-0.3548	-0.0027	-0.2003	-1.0442	0.9775	-0.7228	-1.2034
-1.3553	-0.3854	-1.4227	1.7290	0.7316	0.2531	-1.4900

Columns 15 through 21

0.0392	-0.1468	-0.0198	0.2012	-0.4357	0.0108	-0.0449
-1.0089	-0.4127	-0.8799	0.5255	-1.0989	-0.4742	-0.6783
0.2997	0.4256	0.6892	-0.1704	0.8726	-0.0203	0.1180
0.6210	1.0954	-1.9407	0.2896	1.5091	-0.7880	0.5451
1.0726	-0.2837	-1.4759	1.5632	-0.3636	-1.1859	1.5613
-0.2283	-0.2317	0.4223	0.3896	-0.5429	0.0884	0.0201
-0.2043	-0.2694	-0.1676	0.2632	0.3617	-0.5948	-0.0723
-0.0365	-0.5441	-0.4750	-0.4480	-0.6881	-0.4746	-0.7865
-0.8624	-0.2570	1.2159	1.6124	1.0144	0.3667	-0.7992

Columns 22 through 28

-0.2602	-0.1514	-0.0591	-0.5249	-0.1001	-0.0668	-0.3071
-0.7722	-0.4405	-0.4783	0.1422	-0.0324	0.9236	-0.3892
-0.1163	0.4848	0.2305	0.1438	0.2732	0.0927	0.3401
1.2312	-1.1187	0.3375	1.6606	-0.0280	0.9444	2.5016
-0.5115	0.2395	1.4807	-0.1937	0.7012	0.4081	-0.2519
-0.0982	0.1851	0.1720	0.0278	0.1930	0.0812	-0.2950
-0.0676	0.0020	0.4021	-0.0300	-0.5545	-0.5582	0.0947
0.1436	-0.7380	-0.7710	-0.6133	-0.6861	0.9242	-0.5875
0.1552	0.5865	0.4537	0.6174	1.1963	-0.1149	0.8880

Columns 29 through 30

-0.1742	0.2265
-0.6564	-1.1679
1.1624	0.2859
-1.2073	0.5666
0.0228	0.9671
0.3395	0.0209
-1.1591	-0.0423
-0.3808	0.3940
-0.9474	-0.5041

SHIFT AND PROPAGATE PARAMETERS (2 of 2)

W2 =

Columns 1 through 7

-1.1118 -3.5790 -2.1850 -2.9365 3.8081 -1.0371 -2.0264

Columns 8 through 9

3.3284 4.1655

B1 =

0.5335
-0.4086
0.1243
-0.6208
-0.9886
0.2876
-0.4304
0.2425
1.2105

B2 =

-0.4554

Appendix B:

Typical Mission Profile File

An Example Thrust Level Schedule
Test 2485

Time (sec)	Thrust Level(%)
0	0
5	100
10	100
10	104
60	104
67	100
80	100

Appendix C:

Related Test Results

PROPAGATION RESULTS

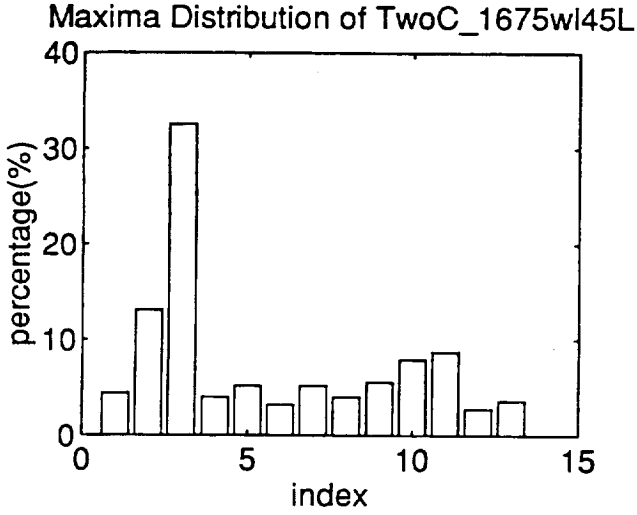

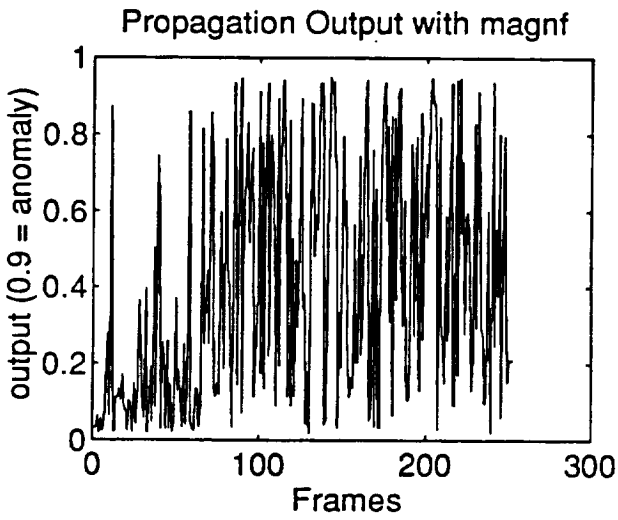

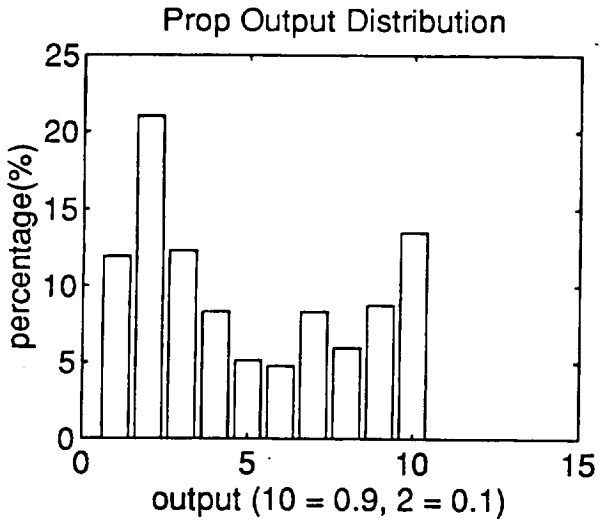

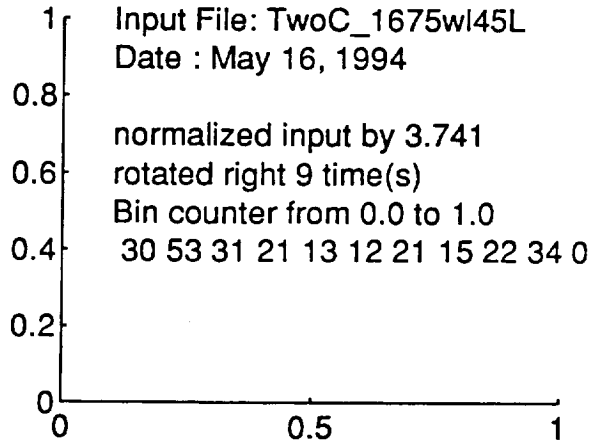

PROPAGATION RESULTS

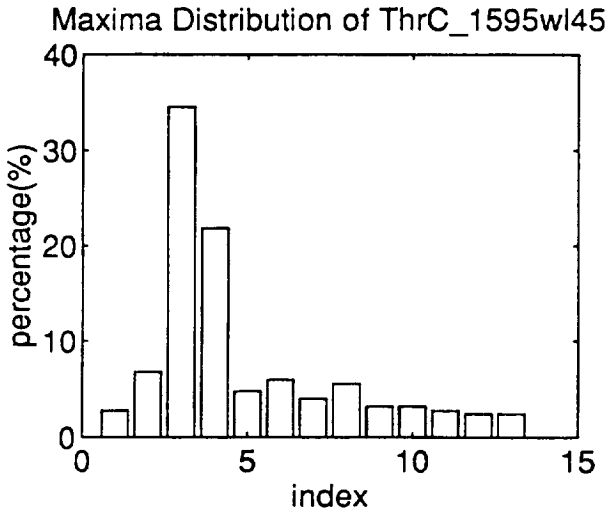

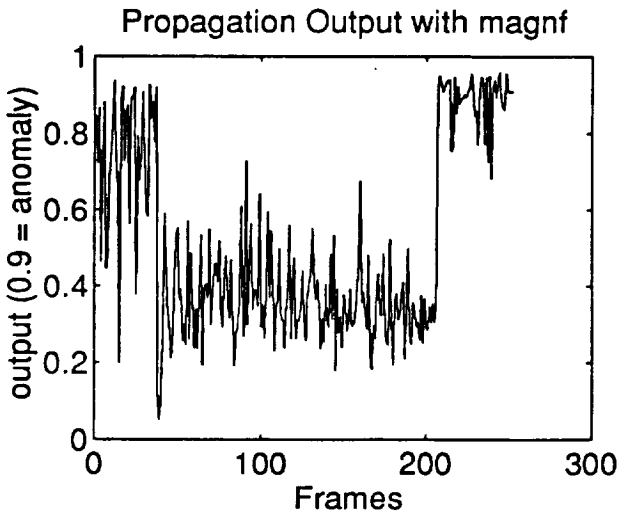

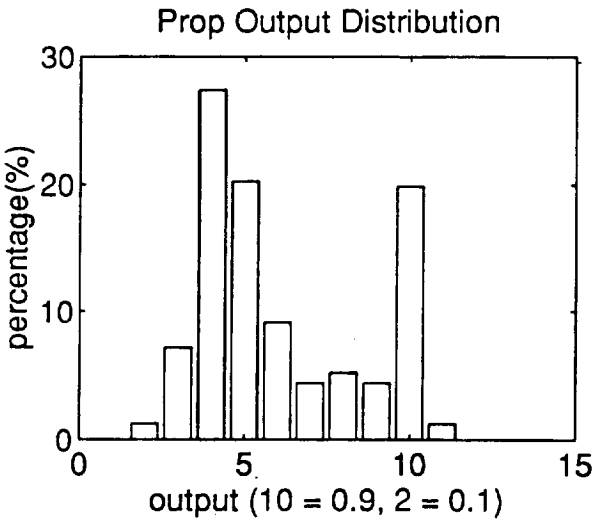

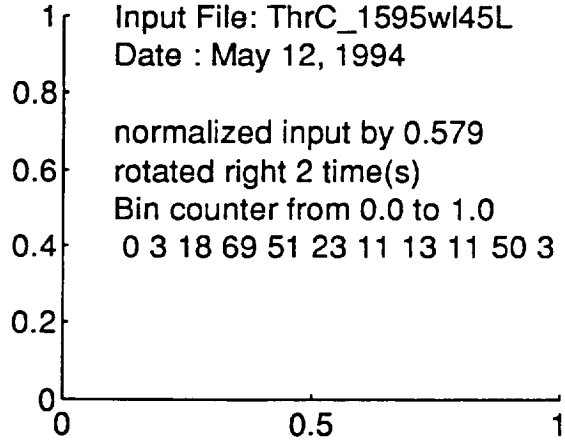

PROPAGATION RESULTS

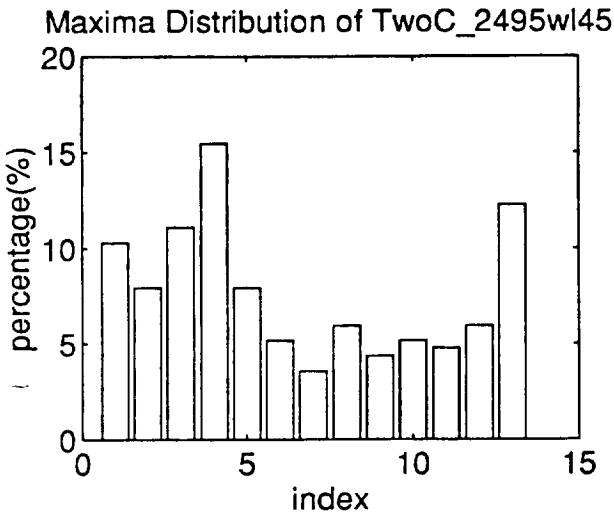

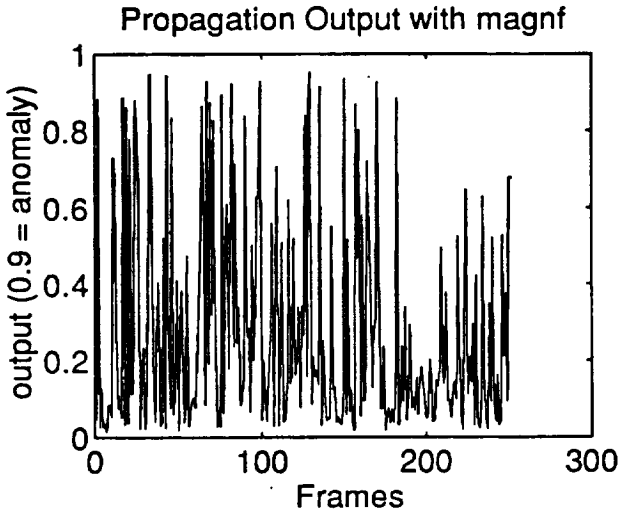

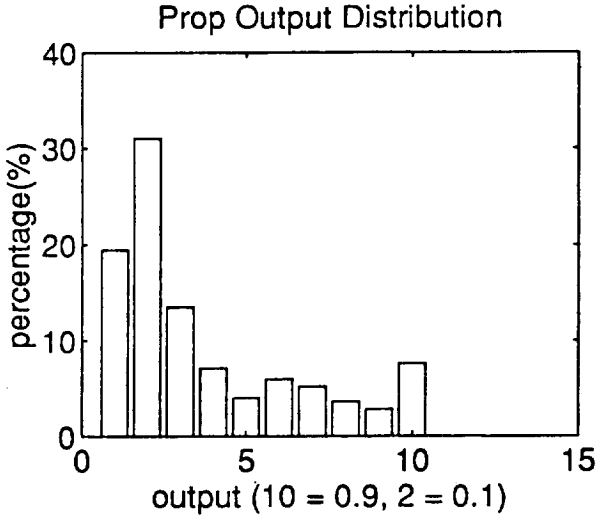

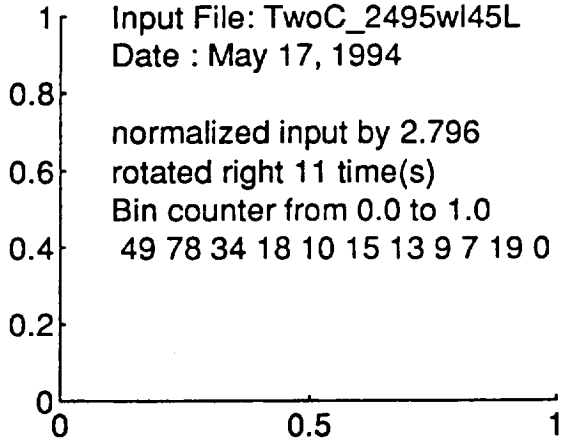

PROPAGATION RESULTS

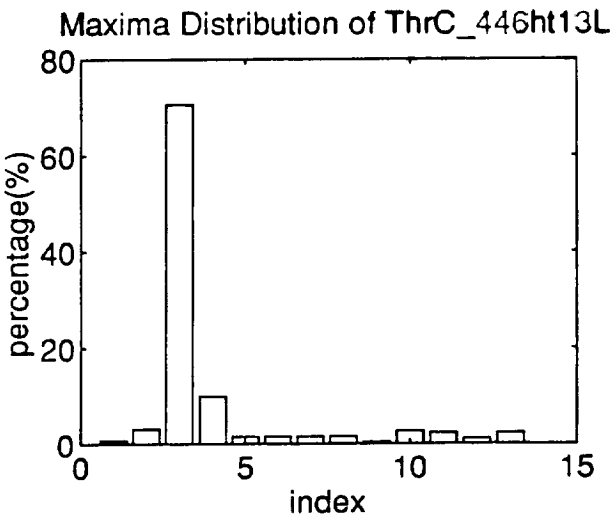

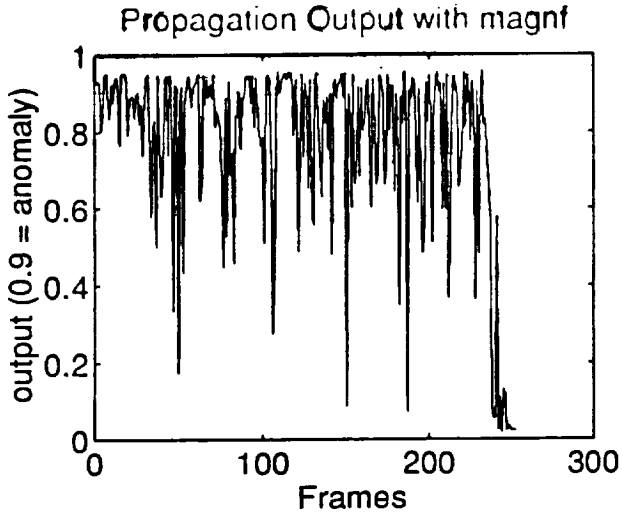

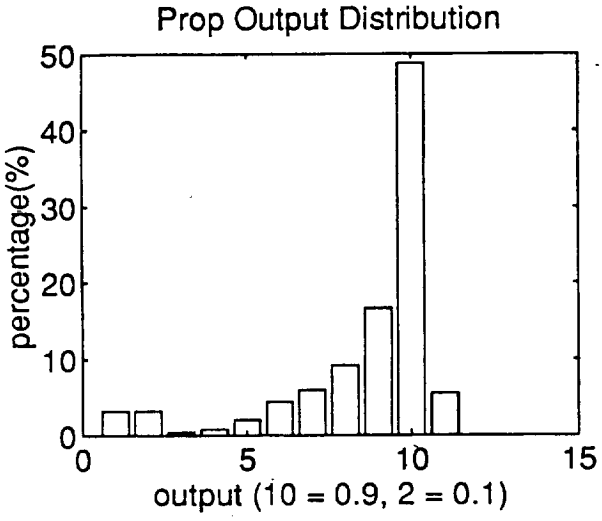

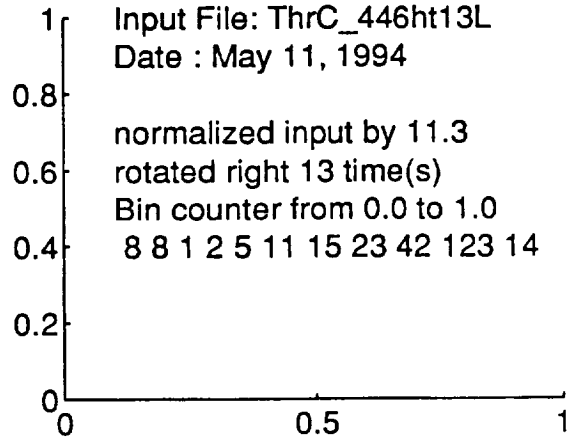

Abbreviations and Acronyms

2C	second harmonic cage frequency
3c	third harmonic cage frequency
ANN	artificial neural networks
EEG	electroencephalogram
HPOTP	high pressure oxygen turbopump
MSFC	Marshall Space Flight Center
NASA	National Aeronautics and Space Administration
SF	synchronous frequency
SSME	space shuttle main engine

References

Hine, M. J., "Absolute Ball Bearing Wear Measurements From SSME Turbopump Dynamic Signals", *Journal of Sound and Vibration* 1989 128(2), pp321-331

Kidd, A., Welbank, M., *Expert Systems: State of Art Report*, Chapter 7,. Pergamon Infotech Limited, 1984, p73.

Kim, J. H., Kissel, R., *Vehicle Health Management using Adaptive Techniques - CDDF Final Rerport* (No. 92-12), NASA TM-108472, 1994.

Kosko, B. , *Neural Networks and Fuzzy Systems*, Pretice Hall, 1992.

McFadden, P.D., Smith, J. D., Model for the Vibration Produced by a Single Point Defect in a Rolling Element Bearing, *Journal of Sound and Vibration*, 1984, 96(1), pp69-82.

Pearson, E.S, Hartley, H.O., *Biometrica Tables for Stasticians*, Vol 1, Third Ed., Cambridge, 1966.

Sunnersjo, C. S., "Rolling Bearing Vibrations - The effect of geometrical imperfections and wear," *Journal of Sound and Vibration* (1985), 98(4), pp455-474.

Weaver, H. J., *Applications of Discrete and Continuous Fourier Analysis*, pp340-346, John Wiley and Sons, 1983.

Bibliography

Kandel, E.R., Hawkins, R.D., "The biological basis of learning and individuality", Scientific American, Special Issue: Mind and Brain, 1992, pp79-86.

Brainbridge, L., The Process Controller in : W. T. Singleton *The Study of Real Skills*, Academic Press, New York, 1976.

Dietz, W.E., Kiech, E.L., Ali, M., "Jet and Rocket Engine Fault Diagnosis in Real Time," Journal of Neural Network Computing, Vol. 1, No. 1, 1989, pp 5-18.

Duyar,A., Merrill, W., "Fault Diagnosis for the Space Shuttle Main Engine," Journal of Guidnance, Control, and Dynamics, Vol 15, No. 2, March-April 1992, pp384-389.

Horak, D. T., "Failure Detection in Dynamics System with Modeling Error," Journal of Guidance, Vol 11, No. 6, pp508-571.

Kakagi, T., Sugeno, M., Fuzzy Identification of Systems and Its Applications to Modeling and Control, IEEE Transactions on Systems, Man, and Cybernetics (SMC), Vol SMC-15, No.1, Jan-Feb 1985, pp116-132.

Merill, W., DeLaat, J, Bruton, W., "Advanced Detection, Isolation, and Accommodation of Sensor Failures - Real-Time Evalution," Journal of Guidance, Vol 11, No. 6, Nov-Dec. 1988, pp517-524.

Negoita, C. V., Expert Systems and Fuzzy Systems, The Benjamin/Cummings Publishing Co. Inc., 1985, QA76.9E96 N384 1985.

Sugeno, M., Kang, G., Structure Identification of Fuzzy Model, Fuzzy Set and Systems 28, 1988, pp15-33.

Sugeno, M., Tanaka, K., "Successive identification of a fuzzy model and its application to prediction of a complex system," Fuzzy sets and Systems 42 (1991), North-Holland, 1991, pp315-334.

Sugeno, M., Kang. G., Fuzzy Modeling and Control of Multilayer Incinerator, Fuzzy Set and System 18, 1986, pp326-346.

Tong, R. M., A Control Engineering Review of Fuzzy Systems, Automatica, Vol. 13, pp 559 - 569.

Scientific American, Special Issue, 1992, Mind and Brain.